# 國 立 交 通 大 學

## 光電工程研究所
## 博 士 論 文

線狀液晶光學圖像形成之研究

**Study on the Optical Pattern Formation through**

**Nematic Liquid Crystal Films**

研究生：徐旭寬

指導教授：王淑霞 教授

賴暎杰 教授

中 華 民 國 九 十 三 年 六 月

線狀液晶光學圖像形成之研究

# Study on the Optical Pattern Formation through

# Nematic Liquid Crystal Films

研究生：徐旭寬　　　　　　Student: Hsu-Kuan Hsu

指導教授：王淑霞 教授　　　Advisor: Prof. Shu-Hsia Chen

　　　　　賴暎杰 教授　　　　　　　Prof. Yinchieh Lai

國 立 交 通 大 學 電 機 資 訊 學 院

光 電 工 程 研 究 所

博 士 論 文

**A Dissertation**

**Submitted to Institute of Electro-Optical Engineering**

**College of Electrical Engineering and Computer Science**

**National Chiao Tung University**

**in Partial Fulfillment of the Requirements**

**for the Degree of**

**Doctor of Philosophy**

**in**

**Electro-Optical Engineering**

**June 2004**

**Hsinchu, Taiwan, Republic of China**

中 華 民 國 九 十 三 年 六 月

# 線狀液晶光學圖像形成之研究

研究生：徐旭寬　　　　　　指導教授：王淑霞 教授

賴暎杰 教授

## 國立交通大學光電工程研究所

## 摘 要

近十年來，非線性光學系統中光學圖像形成的研究吸引了很多學者投入心思探討。在這些研究中，理論的分析和模擬大致可以分為兩大類的光學系統，一為被動系統，一為光學共振腔系統；本論文將針對被動非線性光學系統中的光學圖像形成加以探討。被動光學系統指的是由外場驅動的光學系統，理想來說是穩定且固定的，並沒有考慮到例如光學共振腔中的居數反轉的現象。由於外場和非線性材料的作用，在系統存在微擾或雜訊時，透過強大的非線性作用，外場原本的狀態會受到雜訊的微擾而變得不穩定，因而造成光學圖像的產生。

在本論文中，我們探討利用外加似靜電場偏壓的線狀液晶在單一光回饋的系統中，其光學圖像形成的特性，雖然在此單一光回饋系統中光學圖像形成的穩定和控制已有很多的研究，但是線狀液晶基本的物理特性對於此光學圖像形成的現象影響尚未有深入的探討。在以往利用線狀液晶做此類研究的文獻中，據我們所知並無考慮電場效應的影響，是故我們針對在外加電壓偏壓下的線狀液晶其本身物理非等向特性，研究此光學圖像形成現象的影響。在理論分面，我們根據線狀液晶連續體理論，藉由系統最低能量的 Euler-Lagrange 分析步驟過程中推導出液晶分子

在外場條件下的橫向分佈之擴散方程，根據此擴散方程，我們可以明顯看出液晶本身的彈性非等向性會造成擴散方程中擴散長度的非等向性；針對此系統的擴散方程作線性穩定性分析，我們可以得到光學圖像形成所需的臨界入射光強度，分析此臨界光強我們發現擴散長度的非等向性也會造成臨界光強在橫截面分佈的非等向特性。在外加電場偏壓下的線狀液晶樣品，由於其本身的介電非等向性，液晶分子的排列可以利用外加電場加以適當地控制。在理論分析中，我們發現擴散長度和系統的非線性強度會和液晶分子的分佈有關。

所以，考慮液晶的彈性非等向性及液晶分子分佈的可電調特性，我們提出了不外加傅立葉空間濾波器的條件下，利用液晶本身非等向性造成臨界光強度非等向的特性，簡單地控制入射光強，即可得到條狀和六角狀的光學圖像。此外，由於彈性非等向性會造成臨界光強分佈的非等向性，所以我們更針對液晶法蘭克彈性常數的相對值對此光學圖像之形成會有哪些更進一步的影響作更深入的理論分析。另一方面，由於系統的非線性強度會和液晶分子的分佈有很大的關係，所以我們也就外加偏壓對系統非線性強度的影響作了進一步的分析。考慮電壓和臨界光強度非等向分佈的特性，我們更提出了在適當單一入射光強下，藉由電壓控制系統的非線性強度調變臨界光強的分佈曲線，也可以得到條狀和六角狀的光學圖像的證據。

在理論分析中我們所提出的圖像形成特性，不論是利用控制入射光強或是電壓調變臨界光強分佈的方法，皆可以實驗加以印證。我們的實驗結果也可定性的和理論分析相符。

# Study on the Optical Pattern Formation through

# Nematic Liquid Crystal Films

Student: Hsu-Kuan Hsu                    Advisor: Prof. Shu-Hsia Chen

                                                Prof. Yinchieh Lai

Institute of Electro-Optical Engineering

National Chiao Tung University

## Abstract

Optical pattern formation in nonlinear optical systems has been widely studied in the last decade. Analysis and simulations of pattern formation in two classes of systems are presented. These are passive systems and the cavity systems. Here, we focus on the pattern formation in passive nonlinear optical systems. Passiveness means that the excitation is driven by an externally field, smoothly and constantly in the ideal case, rather than through population inversion. Optical pattern formation results from the nonlinear interaction between the external field and the nonlinear materials. Once a perturbation exists in this nonlinear system, such as the scattering light or the noise, the initial state of the external field may be perturbed and become unstable through the high nonlinearity of the system.

In this dissertation, we investigate the optical pattern formation phenomena by using the quasi-static electric-field-biased liquid crystal

(NLC) films in combination with the one-feedback-mirror system proposed by Firth and Pare. Though the controlling and stabilizing methods have been widely studied the basic physical uniqueness of the nematic liquid crystals appeared in these optical pattern formation phenomena has not been explored very clearly. The governing diffusion-like equation of the optical field induced phase variation in the transverse plane used in most theoretical analysis is assumed to be isotropic based on Firth's method. However, the diffusion-like equation should be modified when nematic liquid crystals are used. Unlike the previously used operating modes such as the hybrid-aligned films, the vertically aligned films or the liquid crystal light valve (LCLV) samples, we further consider the parallelly planar-aligned NLC films biased by a quasi-static electric field. To our knowledge, the electric field effect on the optical pattern formation phenomena has not been included in the earlier theoretical analysis. From our previous works, we know that the optical nonlinearity of such NLC films can be effectively modulated by suitably applying a quasi-static electric field.

Therefore, considering the anisotropic properties of the nematic liquid crystals, we derive the governing diffusion-like equation for the optical field induced phase variation in the transverse plane. Furthermore, the threshold intensity distribution for the patterns to be formed is also derived by the results of the linear stability analysis (LSA) of the governing diffusion-like equation. By analyzing the anisotropic threshold intensity distribution we propose a possible method to obtain the roll and the hexagon patterns without canceling the anisotropic property of the threshold intensity. We successfully observe the roll and the hexagon patterns by simply controlling the input light intensity. Furthermore, from the theoretical analysis, we know that the anisotropic distribution of the

threshold intensity results from the elastic anisotropy of the nematic liquid crystals. Hence, we analyze the issue of how the elastic anisotropy affects the optical pattern formation phenomena. From the results of the analysis of the effects of the elastic anisotropy, we further study the influence of the applied electric field. The nonlinearity of the system can, indeed, be modulated by the applied electric field through the modulation of the orientation of the liquid crystal molecules electrically. Therefore, a simple electric-method is achieved to obtain different optical patterns with a single input light intensity. The experimental results in our work qualitatively agree with the theoretical results well and the suggested pattern-forming properties in our theoretical analysis can be reasonably proved.

# 致謝

不知不覺在交大已是第六個年頭, 此時此刻也將為博士生求學生涯劃下一個句點。鳳凰花開, 和風徐徐, 伴著我邁向人生的下一個階段。求學階段中苦樂交織, 感謝我的雙親徐添貴先生與胡秀銀女士, 長久以來給予我支持與鼓勵, 也讓我無後顧之憂的完成我的學業。 感謝我敬愛的大姊, 二姊和姊夫, 無時無刻的為我打氣。家人的支持與鼓勵是我完成學業的最大支柱, 謝謝你們。

踏進交大, 多年來在我的指導教授王淑霞老師的教導下讓我於人生的課題上得到許多的啟發, 不僅僅是在專業的學術領域研究上讓我有更深入的了解, 更重要的是王老師的一字一句與諄諄教誨對我為人處世有深刻的影響。 感謝您,我人生的導師！

感謝傅永貴教授, 是您帶我進入了光學的世界, 感謝賴暎杰教授, 您親切的指導讓我能堅持下去。 感謝大師兄吳俊傑教授, 大師姊梁寶芝教授, 有了你們的建議與幫忙, 我才得以完成我的論文。 李偉教授, 感謝您在我低潮時都適時拉了我一把, 您的鼓勵感懷於心。

實驗室的眾多學長姊, 同學和學弟妹們, 謝謝你們讓我的研究生生活充滿了挑戰和歡樂。毓仁學長, 慶逸學長, 伯綸學長, 立宜學長, 秋蓮學姊感謝你們給了我很多寶貴的意見與協助。 景翔學長, 勇勳學長, 仰恩學長, 鵲如學姊, 志成學長感謝你們讓我能很快適應研究生的生活。我的同學們菱芝, 傅丞, 建賢感謝你們給我快樂的研究生活與回憶。 怡欣, 您長久來的鼓勵是我非常感激的。佳成, 信全, 乾煌, 揚宜, 彥廷, 梓傑, 朝旭, 惠雯, 英豪, 德源, 建宏, 世郁, 美琪, 品發, 庭毅, 瑞傑謝謝你們豐富了我的研究生活。 勇兒, 夏青, 庭瑞, 葦俐謝謝你們長久以來的照顧和關懷, 有你們的鼓勵讓我堅持下去完成我的論文。范姜, 舒展我志同道合的學弟們, 謝謝你們！俊雄, 怡安, 芝珊學姊謝謝你們幫了我很多忙, 讓我在最後的關鍵時刻可以專心完成工作。

感謝我生命中的好友知己們, ouch, 正桑, 小莉, 逸凱, blue, daff 謝謝你們的鼓勵, 最後, 感謝我生命中最重要的伴侶, 筱慧, 謝謝你一路陪著我, 陪我哀傷, 陪我快樂, 一直以來都默默付出與承受, 感謝您~

新竹國立交通大學

民國九十三年六月　　　　　　　　　　　　　　　　　　　　　　　　徐旭寬

# Table of contents

# List of Figures and Tables

# List of Symbols

$\hat{\boldsymbol{n}}$       molecular director

**P**       polarization of vector form

**E**       electric field of vector form

$\chi^{(i)}$       susceptibility of $i$-th order

n       refractive index

NLC       nematic liquid crystal

LCLV       liquid crystal light valve

LSA       linear stability analysis

θ       orientation of liquid crystal molecules

$n_e$, $n_o$       extraordinary and ordinary refractive indices

$\varepsilon_{//}$, $\varepsilon_{\perp}$       dielectric constants, parallel and perpendicular to molecular

           director

d       cell thickness

ITO       indium tin oxide

L       feedback length

$f$       total free energy density

$f_d$       free energy density for elastic deformation

$f_e$       free energy density for electric term

$f_{op}$       free energy density for optical term

$k_{11}$     splay elastic constant

$k_{22}$     twist elastic constant

$k_{33}$     bend elastic constant

**D**     electric displacement of vector form

**H**     magnetic field of vector form

**B**     magnetic induction of vector form

$k$     $k = (k_{33}/k_{11}) - 1$

$k^*$     $k^* = (k_{11}/k_{33}) - 1$

$w$     $w = 1 - \varepsilon_{//}/\varepsilon_{\perp}$

$\mu$     $\mu = 1 - (n_e/n_o)^2$

$I$     input light intensity

$\theta_a$     average tilt angle

$\theta_p$     optically modulating amplitude

$\theta_t$     transverse orientational angle in the middle layer of the liquid

crystal cell

$\gamma$     viscosity coefficient

$V$     root mean square value of the biased voltage

$l_i$     diffusion length in the i direction

$J_i(2\theta_t)$     Bessel function of the first kind of order $i$

$I_{fr}$     Freedericksz optical intensity

$V_{th}$       Freedericksz voltage

$n_{eff}$       effective index of refraction

$\tau$       response time

$\delta\phi(x, y)$   Kerr induced optical phase variation

$\alpha$       effective nonlinear coefficient

$\rho$       perturbation amplitude

$E_0$       incident plane wave

$E_f$       optical beam just after the NLC film

$q$       wave-vector

$\varphi$       azimuthal angle

$E_b$       reflected beam on the NLC film

$r$       mirror reflectance

$u$       spatial frequency in the x direction

$v$       spatial frequency in the y direction

$u_0$       spatial frequency of the phase grating in the x direction

$v_0$       spatial frequency of the phase grating in the y direction

$\Lambda x$       phase grating spatial period in the x direction

$\Lambda y$       phase grating spatial period in the y direction

$\beta_a$       average polar angle

$k_a$       $k_a=(k_{33}/k_{11})-1$

$k_a^*$       $k_a^*=(k_{11}/k_{33})-1$

$k_b$ $\quad\quad$ $k_b = (k_{22}/k_{11}) - 1$

$k_b^*$ $\quad\quad$ $k_b^* = (k_{22}/k_{33}) - 1$

σ $\quad\quad$ effective diffusion anisotropy parameter

$m$ $\quad\quad$ $\boldsymbol{m} = \dfrac{1}{2}(1 + 2\boldsymbol{J}_0(2\theta_a) - \dfrac{\boldsymbol{J}_1(2\theta_a)}{\theta_a})$

R $\quad\quad$ mirror reflectivity

$\lambda_0$ $\quad\quad$ optical wave length in vacuum

# Chapter 1   Introduction

## 1-1   Overview

In this dissertation, liquid crystals are classified by utilizing the classification scheme of De Gennes and Prost [1], and we will give a brief description of thermotropic liquid crystals. Furthermore, the optical properties of nematics are mentioned briefly.

## 1-1-1   Types of liquid crystals

Liquid crystals are beautiful and unique materials. The term *liquid crystal* signifies a state that is intermediate between the crystalline solid and the amorphous liquid. As a rule, a substance in this state is strongly anisotropic in some of its properties and yet exhibits a certain degree of fluidity. The first observations of liquid crystalline or *mesomorphic* behavior were made towards the end of the nineteenth century by Reinitzer [2] and Lehmann [3] (*mesomorphic*: of intermediate form). Several thousands of organic compounds are known now to form liquid crystals. An essential requirement for mesomorphism to occur is that the molecule must be highly geometrically anisotropic in shape, like a rod or a disc. Depending on the detailed molecular structure, the system may pass through one or more mesophases before it is transformed into the isotropic liquids. Transitions to these intermediate states may be brought about by thermal processes (thermotropic mesomorphism) or by the influence of solvents (lyotropic mesomorphism). Therefore, utilizing the classification scheme of liquid crystal by P. G. De Gennes and J. Prost [1],

there are four major types of liquid crystals: (i) thermotropic, (ii) lyotropic, (iii) polymer and (iv) amphiphilic compounds.

Among these four types, the molecules of the thermotropic liquid crystals are small organic molecules, either rod-like or disk-like, for which an amphiphilic character may or may not be crucial. The simplest way to induce a transition is to vary the temperature therefore they are commonly called thermotropic. Lyotropic liquid crystals are made up of two or more components. Generally, one of them is an amphiphile and another is water. A familiar example of such a system is soap in water. Here the temperature effects are difficult to control, and the nature parameter which one can adjust to induce phase transition is the concentration of the components. Lyotropic liquid crystals are receiving increasing scientific and technological attention because of the way they reflect the unique properties of their constituent molecules. Considering the main-chain or side-chain polymers that are thermotropic mesogens, aside from temperature the molecule weight may also be considered as a variable. Polymeric liquid crystals are potential candidates for electronic devices and ultra-high-strength materials. Amphiphilc compounds may give rise to associations and to mesomorphic behavior, either in the presence of selective solvent or as a pure phase. Thus, depending upon which of the above conditions holds, amphiphilic compounds may be lyotropic or thermotropic.

## 1-1-2   The thermotropic liquid crystals

The well-known, widely used, and extensively studied for their linear as

well as the nonlinear optical properties are thermotropic liquid crystals. In this dissertation, only thermotropic materials are concerned. Thermotropic liquid crystal phases are observed in pure compounds and mixtures. As the temperature increases, these compounds go through a series of phase transitions: from solid to liquid crystal, to isotropic liquid, and finally to vapor phase. Following the nomenclature proposed originally by Friedel [4], thermotropic liquid crystals are classified broadly into three types: nematic, cholesteric and smectic, as shown in Fig. 1.1.



nematic                    cholesteric                    smectic-A
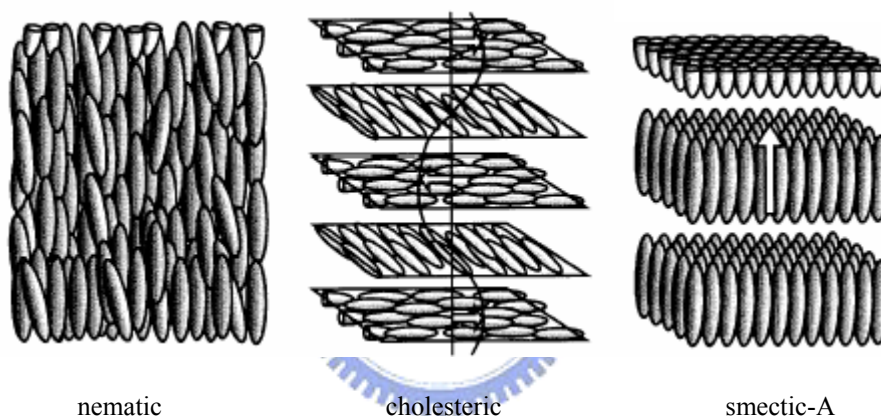
Fig. 1.1    The schematic molecules arrangement of nematics, cholesterics and smectic-A liquid crystals

The nematic phase has a high degree of long-range orientational order of the molecules, but no long-range translational order. The aligned nematic liquid crystal molecules, on the average, are characterized by one symmetry axis, call the director $\hat{n}$. The direction of $\hat{n}$ is arbitrary in space and the state of director $\hat{n}$ and $-\hat{n}$ are indistinguishable. The director can be reoriented by an external field, such as electric field, magnetic field or optical field.

Cholesteric liquid crystal is thermodynamically equivalent to a nematic

except for the chial-induced twist in the directors, as shown in Fig. 1.1. This property results from the synthesis of cholesteric liquid crystals; they are obtained by adding a chiral molecule to a nematic liquid crystal. Some materials, such as cholesteric esters, are naturally chiral. The helical structure can result in selective reflection in wavelength and circular polarizations. The polarization states of the reflected and transmitted waves depend on the pitch length of the cholesteric. Cholesteric liquid crystals have found important applications in areas such as laser cavity mirrors, color filters, and polymer dispersed cholesteric liquid crystal displays.

Smectic liquid crystals, unlike nematic, possess positional order; that is, the positions of the molecules are correlated in some ordered pattern. Form the structure point of view, all smectics are layered-structured with a well-defined interlayer spacing. Therefore, smectics are more ordered than nematics. For a given material, smectic phases usually occur at temperature below the nematic domain. Several subphases of smectics have been discovered, in accordance with the arrangement or ordering of the molecules and their structural symmetry properties. Here, we only briefly describe basic structures of smectic A, C, and $C^*$ phases as shown in Figs. 1.2(a)-(c).

The scheme diagram of layered structure of a smectic-A liquid crystal is shown in Fig. 1.2(a). In each layer the molecules are positionally random, but directionally ordered with their long axis normal to the layer normal. The system is optically uniaxial and the optical axis is normal to the plane of the layer.
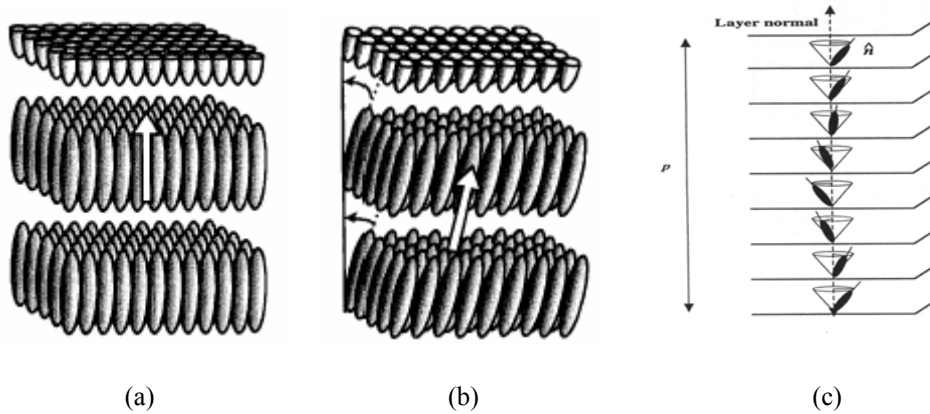
Fig. 1.2    The schematic molecules arrangement of smectic-A, smectic-C and smectic-C$^*$ liquid crystals

The smectic-C phase is a tilted form of smectic-A, i.e., the molecules are inclined with respect to the layer normal. (cf. Fig. 1.2(b)). The smectic-C$^*$ liquid crystals, as depicted in Fig. 1.2(c), is an interesting class of liquid crystal materials. The structure of smectic-C$^*$ is similar to that of smectic-C except for a helical tilt distributions from layer to layer. Another exciting feature of smectic-C$^*$ phase is that it exhibits ferroelectricity. Using this spontaneous polarization, a bistable LC modulator with microsecond response time has been demonstrated in a ferroelectric liquid crystal (FLC) cell.

## 1-2    Nonlinear optics

All optical phenomena occurring in a material arise from the optical field induced polarization **P**. In the electromagnetic theory of light, the material response to the illumination of light is described by the following equation:

$$\mathbf{P} = \chi^{(1)}\mathbf{E} + \chi^{(2)}:\mathbf{EE} + \chi^{(3)}:\mathbf{EEE} + \ldots$$

where **P** is the induced polarization of the material, **E** is the electric field of the light and $\chi^{(1)}$, $\chi^{(2)}$ and $\chi^{(3)}$ are the first-, second- and third-order susceptibilities, respectively. For low light intensity, the high order terms are very small and the optics is adequately described by the first term $\chi^{(1)}$**E**. Linear optics is described by $\chi^{(1)}$ which is related to the index of refraction by $n^2=1+\chi^{(1)}$. For the early days without laser light sources, the scientist can not obtain a reasonable nonlinear effect since a high intensity and coherent light source is required. In 1961, an early second harmonic generation experiment gave the first experimental confirmation for nonlinear theories. A ruby laser with a wave length at 0.6943 $\mu$ m was focused on the front surface of a crystalline-quartz plate. The emergent radiation was examined with a spectrometer and was found to contain radiation at twice the input light frequency.

After the early second-harmonic generation experiments, the field of nonlinear optics has grown rapidly. Many different nonlinear optical phenomena have been observed. These include wave mixing, optical phase conjugation, stimulated scattering, optical pattern formation etc. As indicated above, these nonlinear optical phenomena require intense laser beam. The intensity requirements become even more stringent for higher order process.

## 1-2-1 General overview of nematic-optical nonlinearities

In linear optical process the physical properties of nematic liquid crystals, such as the molecular structure, the individual or collective molecule

6

orientation, the temperature, the density, the population of the electric levels, and so on, are not affected by the optical fields. The optical properties of nematics can be controlled by some external electric fields; this gives rise to a variety of electro-optical effects which are widely used in many electro-optical displays and image-processing applications.

Nematic liquid crystals are also optically nonlinear materials since their physical properties (molecular orientation, temperature and density) are easily perturbed by such an applied high-intensity optical field. Since commonly used liquid crystal molecules are dielectric anisotropic, a polarized light from a laser can induce a realignment of the molecules in the ordered phase. This results in a change of the index of refraction.

Other commonly occurring mechanisms that give rise to the changes of the refractive index are laser-induced changes in the temperature and the density. These changes can arise from several mechanisms. Elevation in the temperature is a natural consequence of the photo-absorptions and the subsequent processes. In the nematic phase the index of refraction is highly dependent on the temperature, through their dependence of on the order parameters, as well as the density.

## 1-2-2 Optical pattern formation in passive nonlinear optical systems

Optical pattern formation in nonlinear optical systems has been widely studied in the last decade. Analysis and simulations of pattern formation in two classes of systems are presented. These are passive systems and the cavity systems. Here, we focus on the pattern formation in passive

nonlinear optical systems. Passiveness means that the excitation is driven by an externally field, smoothly and constantly in the ideal case, rather than through population inversion. Optical pattern formation results from the nonlinear interaction between the external field and the nonlinear materials. Once a perturbation exists in this nonlinear system, such as the scattering light or the noise, the initial state of the external field may be perturbed and become unstable through the high nonlinearity of the system.

After the instability analysis made by Firth and Pare [5] and the experimental observation of hexagon patterns made by Grynberg [6] using the sodium vapor as the nonlinear material, the optical pattern formation phenomena under two counter-propagating pump-beams condition have been confirmed. In 1990, Firth further proposed and demonstrated the optical pattern formation by using a simple arrangement which places a thin Kerr medium in front of a planar feedback mirror [7]. Using this simple one-feedback-mirror system numerous experiments have been successfully performed by using different materials as the nonlinear medium, such as the atomic vapor, the photorefractive crystals and the liquid crystals. The hexagons are the usual patterns frequently observed in these experiments. To stabilize and select patterns other than the hexagons, one can add a Fourier filter in the feedback route [8-10] or break the rotational symmetry by applying the anisotropic nonlinear medium [11]. Up to now, the use of the liquid crystal light valve combined with a Fourier filter in the feedback route is the most favored choice [12].

## 1-3   A survey of the optical pattern formation in a nematic liquid crystal film in one-feedback-mirror system

Utilizing the one-feedback-mirror mirror system the observation of optical pattern formation by using liquid crystals as the nonlinear materials has been studied for many years. In 1992, R. Macdonald and H. J. Eichler successfully observed the hexagon patterns by using a hybrid-aligned nematic liquid crystal (NLC) cell [13]. In the next year, E. Santamato used a clinic-positioned vertical-aligned NLC cell to perform the experiment and also observed the hexagon patterns [14, 15]. Furthermore, in 1994, Santamato observed the roll patterns by considering the unequal property in the diffusion lengths of the governing diffusion-like equation for this system [11]. By rotating the sample to reduce the anisotropy of the diffusion lengths Santamato obtained the hexagon patterns. Furthermore, by inserting a slit as a filter in the feedback route he also obtained the square-like patterns.

In 1995, using the photosensitive-electrode-coated liquid crystal light valve (LCLV), T. Tschudi performed a detailed study on the pattern formation phenomena [16]. In recent years, Tschudi paid more efforts at the stabilizing and pattern selecting topics by adding a Fourier filter in the feedback route [10, 12]. On the other hand, Santamato successfully observed the optical patterns in a defocusing Kerr-like film by adding dye materials into the nematic materials since in the past time one always obtained the optical patterns in a focusing material [17].

## 1-4    Aim of the research

In this dissertation, we investigate the optical pattern formation phenomena by using the quasi-static electric-field-biased liquid crystal (NLC) films in combination with the one-feedback-mirror system proposed by Firth.

Though the controlling and stabilizing methods have been widely studied, the basic physical uniqueness of the nematic liquid crystals appearing in these optical pattern formation phenomena has not been explored very clearly. The governing diffusion-like equation of the optical-field-induced phase variation in the transverse plane used in most theoretical analysis is assumed to be isotropic based on Firth's method. However, as Santamato mentioned in Ref. 11, the diffusion-like equation should be modified and is anisotropic when nematic liquid crystals are used. Unlike the previously used operating modes, such as the hybrid aligned films, the vertically aligned films or the LCLV samples, we further consider the parallelly planar-aligned NLC films biased by a quasi-static electric field. To our knowledge, the electric field effect on the optical pattern formation phenomena has not been included in the theoretical analysis. From our previous works, we know that the optical nonlinearity for such NLC films can be effectively modulated by suitably applying a quasi-static electric field [18-20].

Therefore, considering the anisotropic properties of the nematic liquid crystals we derive the governing diffusion-like equation for the optical-field-induced phase variation in the transverse plane and the threshold intensity distribution for the patterns to be formed is also

derived by the results of the linear stability analysis (LSA) of the governing diffusion-like equation. By analyzing the anisotropic threshold intensity distribution we propose a possible method to obtained the roll and the hexagon patterns without canceling the anisotropic property of the threshold intensity as Santamato did in Ref. 11. We successfully observe the roll and the hexagon patterns by simply controlling the input light intensity [21].

With the results obtained in Ref. 21, we know that the anisotropic distribution of the threshold intensity is resulted from the elastic anisotropy of the nematic liquid crystals. Therefore, we analyze the issue of how the elastic anisotropy affects the optical pattern formation phenomena [22]. From the results we get in Ref. 22, we further study the influence of the applied electric field. The nonlinearity of this system indeed can be modulated by the applied electric field through the modulation of the orientation of the liquid crystal molecules electrically. Therefore, a simple electric-method to obtain different optical patterns is achieved with a single input light intensity [23].

In the following chapter, a general theoretical description of the governing diffusion-like equation and the analytical results of the threshold intensity for both the parallelly planar-aligned and the vertical-aligned NLC films are presented. In chapter 3, we give a discussion of how the intrinsic anisotropic properties affect the optical pattern formation phenomena. The experimental results concerning a parallelly planar-aligned NLC film are given in chapter 4. Finally, the discussion and conclusion are made in chapter 5.

# Chapter 2   Theory

In this chapter, the general theoretical derivation of the governing diffusion-like equation for the optical-field-induced phase variation and the analytical results of the threshold intensity for the optical pattern formation for both the parallelly planar-aligned and the vertical-aligned NLC films are presented.

## 2-1 Field-induced optical phase variation in the transverse plane when an electric-field-biased liquid crystal film is used

In order to obtain the governing diffusion-like equation for the optical-field-induced phase variation the governing diffusion-like equation for the orientational distribution of the liquid crystal directors in the transverse plane with externally applied fields must be obtained first. We start from the continuum theory for the NLCs. If one assumes a p-polarized light beam impinges on an electric-field-biased liquid crystal film, then the liquid crystal directors will be reoriented when the electric and the optical fields are high enough. As the liquid crystal directors are reorientated, the light beam passing through the liquid crystal film will experience a phase delay according to the orientational distribution of the liquid crystal directors. Therefore, the orientational

distribution of the liquid crystal directors $\theta(x, y, z)$ must be calculated first.

Fig. 2.1 shows the configuration of the quasi-static electric-field-biased planar-aligned homogeneous NLC film considered in our derivation and Fig. 2.2 shows the geometric scheme of our one-feedback-mirror system for observing the optical pattern formation phenomena. The nematic material is assumed to have positive optical and dielectric anisotropies, namely $n_e > n_o$ and $\varepsilon_{//} > \varepsilon_{\perp}$ where n and $\varepsilon$ denote the refractive indices and dielectric constants, and the subscripts refer to the directions parallel and perpendicular to the director, respectively.
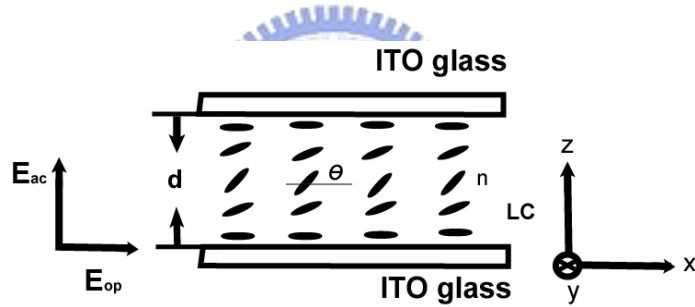


Fig. 2.1    The planar-aligned nematic liquid crystal cell: LC, liquid crystal; θ, molecular orientational angle; E$_{op}$ , optical field; E$_{ac}$, electric field; $\hat{n}$ , molecular director; d, cell thickness, and ITO, indium tin oxide.

A quasi-static electric field is applied along the z-axis and is perpendicular to the unperturbed director $\hat{n}$. A p-polarized light impinges on the NLC film with its polarization direction parallel to the easy axis of the liquid crystal directors. After it passing through the NLC sample the light propagates freely to and from the planar feedback mirror and finally impinges on the sample again.
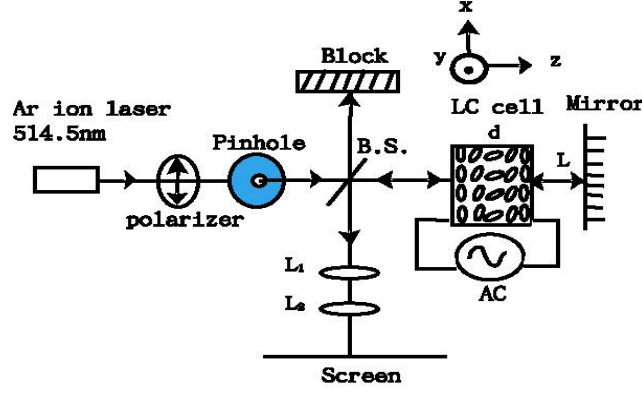
Fig. 2.2 Geometric scheme of the one-feedback-mirror system: B.S., beam splitter; d, cell thickness; L, feedback length; LC, liquid crystal; L'i, lens

In order to obtain the governing diffusion-like equation for the optical field induced phase variation in the transverse plane the orientational distribution of the molecules $\theta(x, y, z)$ should be calculated first. From the continuum theory, which is a macroscopic phenomenological theory of liquid crystals dealing with a slowly varying director field, the orientational distribution function $\theta(x, y, z)$ is obtained by minimizing the total free energy $F = \int f \, dv$. The total free energy density $f$ for our system is

$$f = f_d + f_e + f_{op}, \tag{1}$$

where

$$f_d = \frac{1}{2}[k_{11}(\nabla \bullet \hat{n})^2 + k_{22}(\hat{n} \bullet \nabla \times \hat{n})^2 + k_{33}(\hat{n} \times \nabla \times \hat{n})^2],$$

$$f_e = -\frac{1}{8\pi}E_e \bullet D_e,$$

and

$$f_{op} = -\frac{1}{8\pi}[E_{op} \bullet D_{op} + H_{op} \bullet B_{op}],$$

where $f_d$, $f_e$ and $f_{op}$ represent the elastic deformation, electric, and optical

14

terms, respectively. In these relations, $k_{11}$, $k_{22}$ and $k_{33}$ are the splay, twist, and bend elastic constants, respectively. **E** and **D** represent the electric field and displacement while **H** and **B** are the magnetic field and induction, respectively. Therefore, choose the coordinate system with the z axis perpendicular to the cell walls, the x-y plane coincides with the input cell wall and the $\hat{x}$ direction is along with the easy axis of the liquid crystal directors. Considering the director $\hat{n} = (\cos\theta, 0, \sin\theta)$ the free energy density $f$ can be expressed as

$$f = \frac{1}{2}\{k_{11}[(1+k\cos^2\theta)(\frac{\partial\theta}{\partial x})^2 + (1+k\sin^2\theta)(\frac{\partial\theta}{\partial z})^2 + 2k\sin\theta\cos\theta(\frac{\partial\theta}{\partial x})(\frac{\partial\theta}{\partial z})]$$

$$+ k_{22}(\frac{\partial\theta}{\partial y})^2\} - \frac{D_z^2}{8\pi\varepsilon_\perp(1-w\sin^2\theta)} \frac{In_e}{c(1-\mu\sin^2\theta)^{1/2}} \quad , \tag{2}$$

where $k = (k_{33}/k_{11}) - 1$, $w = 1 - \varepsilon_{//}/\varepsilon_\perp$, $\mu = 1-(n_e/n_o)^2$, $D_z$ is the z component of the electric displacement, c is the velocity of light in vacuum, and $I$ is the input optical intensity. Actually, it's not easy to deal with the three dimensional equation directly. Instead of solving the distribution function $\theta(x, y, z)$ by the Euler–Lagrange equations directly, we assume a trial solution of $\theta(x, y, z)$ as

$$\theta(x, y, z) = [\theta_a + \theta_p(x, y)]\sin(\frac{\pi z}{d})$$

$$= \theta_t(x, y)\sin(\frac{\pi z}{d}) \quad . \tag{3}$$

We also assume the hard-boundary condition, $\theta(z=0)=\theta(z=d)=0$.

Here $d$ is the thickness of the sample and $\theta_a$, $\theta_p$, and $\theta_t$ represent the electrically biased spatial average orientational angle, the optically modulated amplitude, and the transverse orientational angle in the middle layer of the liquid crystal cell, respectively. Substituting Eq. (3) into Eq. (2), integrating the total volume of the cell, and following the Euler-Lagrange optimization process, we can get the torque balance equation of the liquid crystal directors. After some algebra and considering the viscositic term, the torque balance equation can be expressed as

$$\gamma\frac{\partial\theta_t}{\partial t}-l_x^2(\frac{\partial^2\theta_t}{\partial x^2})-l_y^2(\frac{\partial^2\theta_t}{\partial y^2})+\theta_t=[\frac{V^2}{V_{th}^2}-\frac{I}{I_{fr}}+\frac{k}{2}]\frac{2J_1(2\theta_t)}{G}, \qquad (4)$$

with

$$l_x^2=\frac{1}{G}(\frac{d}{\pi})^2\{1+\frac{k}{2}[1+2J_0(2\theta_t)-\frac{J_1(2\theta_t)}{\theta_t}]\},$$

$$l_y^2=\frac{1}{G}(\frac{d}{\pi})^2(\frac{k_{22}}{k_{11}}),$$
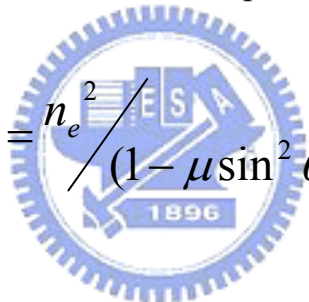
$$G=\{2+k-\frac{k}{2}[J_0(2\theta_t)-J_2(2\theta_t)]\},$$

$$V_{th}=2\pi[\frac{\pi k_{11}}{\varepsilon_{//}-\varepsilon_\perp}]^{\frac{1}{2}},$$

and

$$I_{fr}=ck_{11}(\frac{\pi}{d})^2\frac{1}{(-n_e\mu)}. \qquad (5)$$

Here $\gamma$ is the viscosity coefficient, $V$ is the root-mean-square value of the biased voltage, $l_i$ (i = x, y) is the diffusion length in the i direction, $J_i(2\theta_t)$ is the Bessel function of the first kind of order $i$, and $I_{fr}$ and $V_{th}$ are the Freedericksz optical intensity and voltage. From Eq. (4), one can see that the viscosity term indicates the dynamic behavior of the orientation of NLC directors. Furthermore, the spatial orientation of NLC directors is also related with the spatial distribution of the external fields. Eq. (4) can be changed into the diffusion-like equation for the optical phase variation in the transverse plane since the effective index of refraction for the NLC materials can be expressed as

$$ n_{eff}^{\;2} = n_e^{\;2} \Big/ (1 - \mu \sin^2 \theta) \; , \tag{6} $$

and the optical phase variation in the transverse plane is

$$ \Psi(x,y) = \frac{2\pi}{\lambda_0} \int_0^d n_{eff} \, dz \; . \tag{7} $$

After substituting Eq. (3) into Eq. (6) and replacing $n_{eff}$ in Eq. (7) by Eq. (6), the diffusion-like equation can be expressed as

$$ \tau \frac{\partial \Psi}{\partial t} - l_x^{\;2} \frac{\partial^2 \Psi}{\partial x^2} - l_y^{\;2} \frac{\partial^2 \Psi}{\partial y^2} + \Psi = [\frac{V^2}{V_{th}^{\;2}} - \frac{I}{I_{fr}}]S + T \; . \tag{8} $$

Here $\tau$ is the response time related with the viscosity coefficient, S and T are the coefficients which are functions of the material parameters and the orientation of the liquid crystal directors. Now if we consider a uniform applied voltage, then the phase variation in the transverse plane directly comes from the light intensity variation in the transverse plane. It follows that the constant phase terms and the constant driving forces can be removed from Eq. (8). Therefore a simplified governing diffusion-like equation for the Kerr-induced optical phase variation $\delta\phi(x, y)$ can be obtained and shown as

$$\tau \frac{\partial \delta\phi}{\partial t} - l_x^{\ 2} \frac{\partial^2 \delta\phi}{\partial x^2} - l_y^{\ 2} \frac{\partial^2 \delta\phi}{\partial y^2} + \delta\phi = \alpha\delta I \; ; \tag{9}$$

$$\alpha = - \frac{2\pi n_e \mu d J_1(2\theta_t) J_1(2\theta_a)}{\lambda_0 I_{fr} G} . \tag{10}$$

Eq. (9) is similar to the equation proposed by Firth in Ref.7 except the anisotropic property of the diffusion lengths in the transverse plane and $\alpha$ is the effective nonlinear coefficient affected by the molecular orientations as shown in Eq. (10). From Eq. (5) and Eq. (10), we can see that the relative coefficients can be obtained as the material parameters, the electrically biased spatial average orientational angle $\theta_a$, and the optically modulating amplitude $\theta_p$ are known. The electrically biased spatial average orientational angle $\theta_a$ can be determined by minimizing

the total free energy under the hard boundary condition and the assumption of a uniformly distributed electric field. Following the Euler-Lagrange optimization process, we find that $\theta_a$ has to obey the following equation

$$\theta_a\{2+\frac{k}{2}[2-J_0(2\theta_a)+J_2(2\theta_a)]\}=(\frac{V^2}{V_{th}^2}-\frac{I}{I_{fr}}+\frac{k}{4})2J_1(2\theta_a) . \qquad (11)$$

Eq. (11) can be calculated numerically if d, V, $I$, and the material parameters are all known. From our previous paper [22], the optically modulating amplitude is much smaller than the electrically biased spatial average orientational angle, $\theta_p << \theta_a$. Therefore we can reasonably substitute $\theta_t$ by $\theta_a$ in both Eq. (5) and Eq. (10).
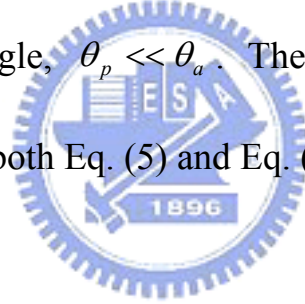
## 2-2　The threshold intensity for patterns to be formed

To obtain the threshold intensity for patterns to be formed, we follow the linear stability analysis (LSA) in Ref. 11. Consider the geometric scheme shown in Fig. 2.2. The incident plane wave $E_0$ passes through the NLC film then propagates freely to and from the reflecting mirror and finally impinges on the NLC film. For such a system, the LSA of Eq. (9) can be performed by assuming that a noise with its azimuthal angle φ on the transverse plane interacts with the input plane wave $E_0$. The noise and $E_0$ interfere with each other which results in the optical intensity

distribution on the transverse plane. Since the NLC molecules possess the dielectric anisotropic property, the orientation of the NLC molecules follows the distribution of the optical intensity. Therefore, when the plane wave passes through the NLC film the plane wave $E_0$ experiences a phase modulation. Now assume a small sinusoidal phase modulation $\delta\phi$ is applied to the forward plane wave $E_0$. After the plane wave $E_0$ just passes through the sample, it will experience the phase variation as given by
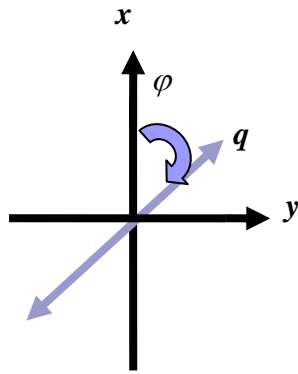


$$\boldsymbol{E}_f(\boldsymbol{x}, \boldsymbol{y}) = \boldsymbol{E}_0\{1 + i\rho\cos[(\boldsymbol{q}\cos\varphi)\boldsymbol{x} + (\boldsymbol{q}\sin\varphi)\boldsymbol{y}]\}$$

$$= E_0\{1 + i\delta\phi\}. \tag{12}$$

Here $\rho \ll 1$ is the perturbation amplitude and the terms related to the wave vector $q$ have been written in the polar form with the azimuthal angle $\varphi$ from the axis of the anisotropy to the wave vector clockwise. The beam $E_f(x, y)$ then propagates freely to and from the reflecting mirror. This part of wave propagation can be readily modeled by the Fresnel propagation formula such as

$$E(x,y,z) = \frac{e^{jkz}}{j\lambda z}e^{j\frac{\pi}{\lambda z}(x^2+y^2)}\iint E_f(x',y')e^{j\frac{\pi}{\lambda z}(x'^2+y'^2)}e^{-j\frac{2\pi}{\lambda z}(xx'+yy')}dx'dy'$$

$$=\frac{e^{jkz}}{j\lambda z}e^{j\frac{\pi}{\lambda z}(x^2+y^2)}F\{U_t(x',y')e^{j\frac{\pi}{\lambda z}(x'^2+y'^2)}\}$$

$$=\frac{e^{jkz}}{j\lambda z}e^{j\frac{\pi}{\lambda z}(x^2+y^2)}F\{E_0[1+i\rho\cos(q_{x'}x'+q_{y'}y')]e^{j\frac{\pi}{\lambda z}(x'^2+y'^2)}\}$$

$$=E_0\frac{e^{jkz}}{j\lambda z}e^{j\frac{\pi}{\lambda z}(x^2+y^2)}F\{[1+\frac{i\rho}{2}(e^{j(q_xx'+q_yy')}+e^{-j(q_xx'+q_yy')})]e^{j\frac{\pi}{\lambda z}(x'^2+y'^2)}\}$$

$$=E_0\frac{e^{jkz}}{j\lambda z}e^{j\frac{\pi}{\lambda z}(x^2+y^2)}\{[\delta(u,v)+\frac{i\rho}{2}(u+u_0,v+v_0)+\frac{i\rho}{2}(u-u_0,v-v_0)]\otimes[(j\lambda z)e^{-j\pi\lambda z(u^2+v^2)}]\}$$

$$=E_0\frac{e^{jkz}}{j\lambda z}e^{j\frac{\pi}{\lambda z}(x^2+y^2)}\{[\delta(u,v)+\frac{i\rho}{2}(u+u_0,v+v_0)+\frac{i\rho}{2}(u-u_0,v-v_0)]\otimes[(j\lambda z)e^{-j\pi\lambda z(u^2+v^2)}]\}$$

$$=E_0e^{jkz}\{1+i\rho e^{-j\pi\lambda z(u_0^2+v_0^2)}\cos[2\pi(u_0x+v_0y)]\}$$

$$=E_0e^{jkz}\{1+i\rho e^{-j\pi\lambda z\frac{q^2}{4\pi^2}}\cos(q_xx+q_yy)\},$$

(13)

where

$$q_x=\frac{2\pi}{\Lambda_x}=q\cos\varphi; q_y=\frac{2\pi}{\Lambda_y}=q\sin\varphi;$$

$$u=\frac{1}{x}; v=\frac{1}{y};$$

$$u_0=\frac{1}{\Lambda_x}; v_0=\frac{1}{\Lambda_y},$$

here $u_0$ and $v_0$ are the spatial frequencies of the phase grating in the x and y directions, respectively. $\Lambda_x$ and $\Lambda_y$ are the spatial period of the grating in the x and y directions, respectively. Then the reflected beam on the film can be expressed as

$$E_b(x,y,2L)=rE_0e^{jk2L}[1+i\rho e^{-j\pi\lambda 2L\frac{q^2}{4\pi^2}}\cos(q_xx+q_yy)]. \quad (14)$$

By squaring the reflected beam field to obtain the feedback intensity distribution which can be expressed as

$$I_b = I_0\{1 - 2R\rho\cos[(q\cos\varphi)x + (q\sin\varphi)y]\sin(\frac{q^2}{2\pi}\lambda_0 L)\}. \qquad (15)$$

Therefore, the total intensity

$$I = I_f + I_b$$

$$= I_0\{(1 + R) - 2R\rho\cos[(q\cos\varphi)x + (q\sin\varphi)y]\sin(\frac{q^2}{2\pi}\lambda_0 L)\},$$

implying that the variational light intensity

$$\delta I = -2RI_0\rho\cos[(q\cos\varphi)x + (q\sin\varphi)y]\sin(\frac{q^2}{2\pi}\lambda_0 L)$$

$$= -2RI_0\sin(\frac{q^2}{2\pi}\lambda_0 L)\delta\phi. \qquad (16)$$

In Eqs. (15) and (16), $L$ is the length between the sample and the reflecting mirror, R is the reflectivity of the reflecting mirror, and $I_0$ is the intensity of the forward beam and is the square of $E_0$. Substituting Eq. (16) into the right side of Eq. (9) for performing the stability analysis, we can derive the following threshold intensity for the growing of the perturbation after some algebra:

$$I_{th}(q,\varphi) = \frac{1 + q^2(l_x^2\cos^2\varphi + l_y^2\sin^2\varphi)}{2R\alpha\sin(\frac{q^2}{2\pi}\lambda_0 L)} \quad . \qquad (17)$$

From Eq. (17), the threshold intensity as a function of $q$ is expected to reach its minimum approximately when $\sin(q^2\lambda_0 L/2\pi)=1$ or equivalently when

$$q \cong \frac{\pi}{\sqrt{\lambda_0 L}} \qquad (18)$$

At this time the net feedback length 2L is simply the required length to transform the phase modulation in Eq. (12) to pure amplitude modulation as the beam is reflected back to the sample ( the Talbot Effect). This can be easily verified from Eq. (14) and the configuration of the Talbot Effect is illustrated in Fig. 2.3.

$$z_{tal} = \frac{8\pi^2}{\lambda q^2} = 2\frac{\Lambda}{\lambda}$$



NM/PM   AM   PM   AM   PM

$\frac{1}{4}z_{tal}$   $\frac{3}{4}z_{tal}$   $z_{tal}$
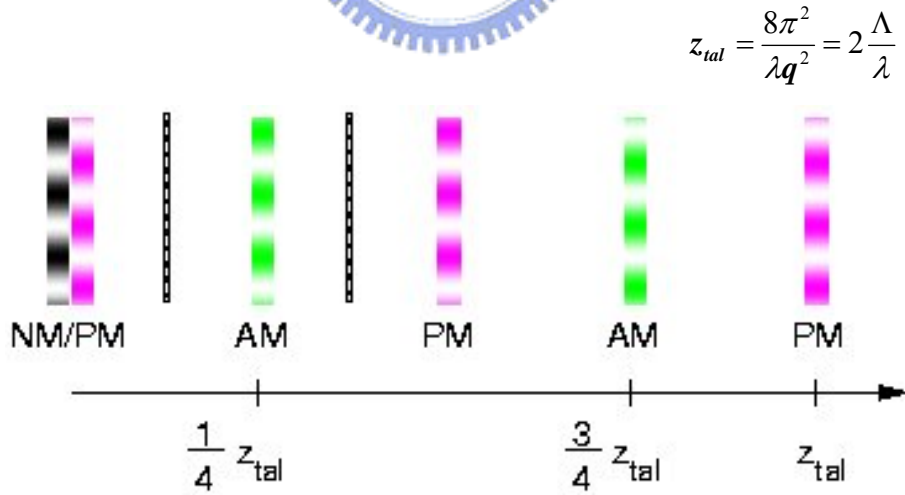
Fig. 2.3    The transferring between the phase modulation and amplitude modulation based on the Talbot Effect ($Z_{tal}$: Talbot length).

Therefore, the threshold intensity in various azimuthal angles can then be readily obtained when the spatial frequency is known.
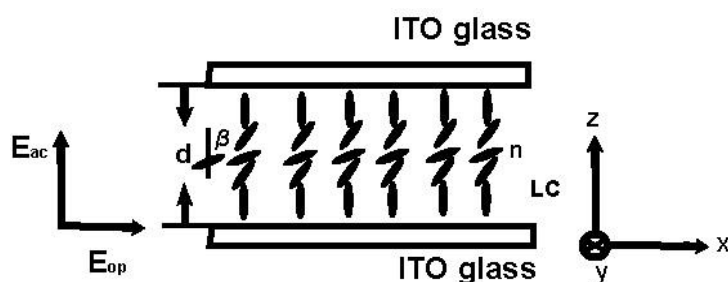


Fig. 2.4   The vertically-aligned nematic liquid crystal cell: LC, liquid crystal; $\beta$, molecular orientational angle; E$_{op}$, optical field; E$_{ac}$, electric field; $\hat{n}$, molecular director; d, cell thickness, and ITO, indium tin oxide.

The derivation of the governing diffusion-like equation and the threshold intensity for the patterns to be formed for the case of the vertical-aligned sample as shown in Fig. 2.4 is the same as we do for the homogeneous sample. The results for the vertical-aligned sample are similar to that for the homogeneous sample and one just needs to change the average tilt angle $\theta_a$, G, k and $k_{11}$ in Eq. (5) by the average polar angle $\beta_a$, $G^* = \{2 + k^*[1-(1/2)[J_0(2\beta_a) - J_2(2\beta_a)]]\}$, $k^* = (k_{11}/k_{33})-1$ and $k_{33}$, respectively.

# Chapter 3　Anisotropy analysis

From the theoretical results of the governing diffusion-like equation and the threshold intensity for the patterns to be formed we can know that when nematic liquid crystals are used as the nonlinear material to perform the optical pattern formation experiment the intrinsic physical properties, such as the optical birefringence, the unequal property of Franck elastic constants, and the dielectric anisotropy, all play important roles in the pattern formation phenomena. In this chapter, we investigate the influence of these anisotropic properties on the pattern formation phenomena and for convenience the parameters used in our numerical analysis are on the basis of the homogeneous E7 cell with its cell gap of 68 μm though the theoretical results hold for other nematic materials.
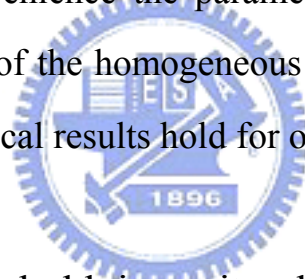
## 3-1　Anisotropic threshold intensity distribution results from the elastic anisotropy of nematic liquid crystals

From Eq. (9) and Eq. (17) we can easily see that the anisotropic nonlinear response of NLC films indeed induces the anisotropic distribution of the needed threshold intensity for the pattern to be formed and from Eq. (5) we can see that the anisotropy of the diffusion lengths comes from the anisotropy of Franck elastic constants. Fig. 3.1(a) shows the theoretical calculated threshold power in various $\theta_a$ when the azimuthal angle is $\varphi = 90^0$, $60^0$ and $0^0$. The threshold power is calculated by the product of the threshold intensity and the beam area. Actually, the key physical

parameter for the optical pattern formation is the intensity and we use the threshold power for the consideration of the practical-experimental reality. From Fig. 3.1(a) we can see that for each fixed $\varphi$ the minimum of the threshold power locates at about $\theta_a = 0.9$ radian. For each fixed $\theta_a$ the smallest threshold power is at $\varphi = 90^0$ and the largest threshold one is at $\varphi = 0^0$ and $180^0$. For convenience in Fig. 3.1(b), we plot the threshold power in various $\varphi$ when $\theta_a$ is kept at 0.787 radian. From Fig. 3.1(b), one can see that the anisotropic property of the threshold power in various azimuthal angles. It's more clear that the minimum threshold power locates at $\varphi = 90^0$ and the maximum one locates at $\varphi = 0^0$ and $180^0$.



(a)

(b)
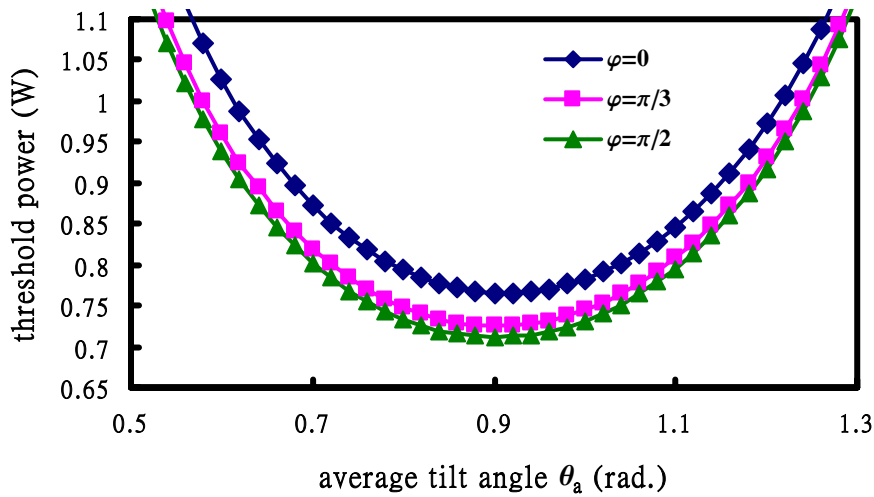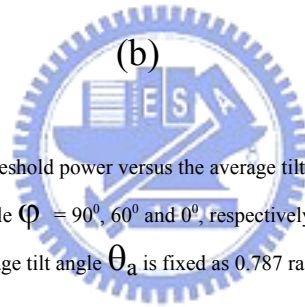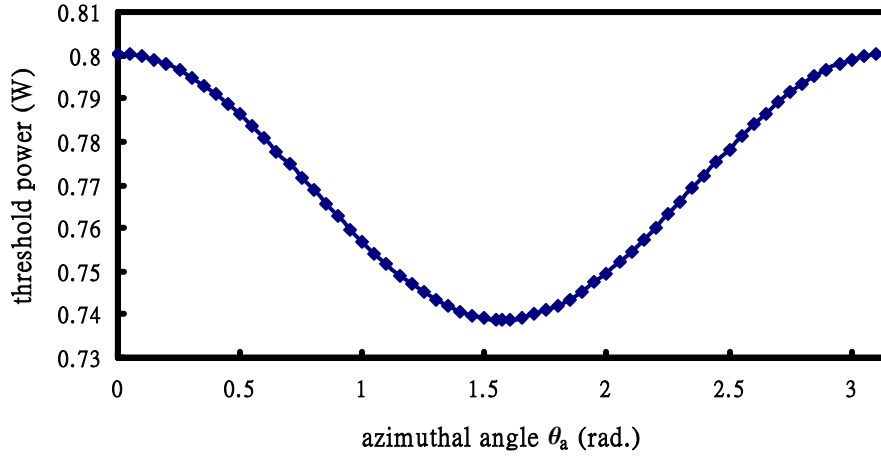
Fig. 3.1 (a) The calculated curves of the threshold power versus the average tilt angle $\theta_a$ when the azimuthal angle $\varphi$ is fixed; from the top to the bottom are azimuthal angle $\varphi = 90^0$, $60^0$ and $0^0$, respectively (b) the calculated curve of the threshold power versus the azimuthal angle $\varphi$ when the average tilt angle $\theta_a$ is fixed as 0.787 rad.

On the basis of this anisotropic distribution of the threshold power, we can propose a method to obtain different optical patterns. The formation of different patterns may be associated with the possibility of the appearance of the modes with different azimuthal angles allowed to exist under the applied input light power and other experimental conditions. When the input light power is above and close to the minimum threshold power, the modes with azimuthal angles close to $\varphi = 90^0$ are allowed to appear. However, these modes will not oscillate to form other patterns since they fulfill no momentum conservation conditions. Therefore, only the mode with the lowest threshold power (in our case the mode with $\varphi =$

$90^0$) will be enhanced and the roll pattern should be observed.

On the other hand, when the input light power is above but not far from the maximum threshold power, all the modes with azimuthal angle from $\varphi = 0^0$ to $\varphi = 360^0$ are allowed to appear. This is similar to that in the isotropic case and we can expect the oscillation of three ripple patterns leading to hexagons formation. This is because the hexagons satisfy the momentum conservation condition and the beams can enhance with each other.

## 3-2    Influence of Frank elastic constant anisotropy on optical pattern formation phenomena
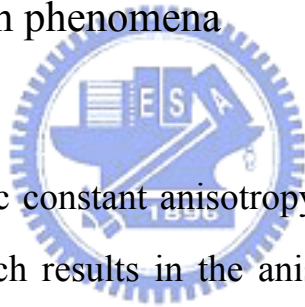
The intrinsic Frank elastic constant anisotropy induces the anisotropy of the diffusion length, which results in the anisotropic distribution of the threshold intensity for optical pattern formation. Therefore, the effects of the elastic constant anisotropy on optical pattern formation are studied in this subsection and the obtained numerical results can reasonably explain the optical patterns that can be formed.

From Eq. (9) one can see that the key factor is the anisotropy of the diffusion lengths. Therefore, in order to clearly analyze the effects of the Franck elastic constants on the pattern formation phenomena we rewrite the parameters in Eq. (5) as

$$l_x^2 = \frac{1}{G}(\frac{d}{\pi})^2(1+mk_a);$$

$$l_y^2 = \frac{1}{G}(\frac{d}{\pi})^2(1+k_b);$$

$$\alpha = -\frac{2\pi n_e \mu d J_1(2\theta_a)^2}{\lambda_0 I_{fr} G};$$

(19)

$$I_{fr} = ck_{11}\frac{(\frac{\pi}{d})^2}{(-n_e\mu)},$$

where

$$G = \{2 + k_a - \frac{k_a}{2}[J_0(2\theta_a) - J_2(2\theta_a)]\};$$

$$m = \frac{1}{2}(1 + 2J_0(2\theta_a) - \frac{J_1(2\theta_a)}{\theta_a});$$

$$k_a = \frac{k_{33}}{k_{11}} - 1;$$

$$k_b = \frac{k_{22}}{k_{11}} - 1;$$

$$\mu = 1 - (\frac{n_e}{n_o})^2,$$

In order to determine the anisotropic property of the threshold intensity distribution, one should calculate the anisotropy of the diffusion lengths first. From Eq. (17), the anisotropy of the diffusion lengths can be expressed as:

$$\Delta l^2 = l_x^2 - l_y^2 = [\frac{1}{G}(\frac{d}{\pi})^2]\sigma$$

(20)

where

$$\sigma = mk_a - k_b$$

(21)

From Eq. (5), the parameter σ can be considered as the effective diffusion

anisotropy parameter. For the vertical-aligned NLC films, the average tilt angle $\theta_a$, the coefficient $G$ and the elastic anisotropies $k_a$ and $k_b$ in the above equations have to be replaced by the average polar angle $\beta_a$,

$$G^* = \{2 + k^*[1 - (1/2)[J_0(2\beta_a) - J_2(2\beta_a)]]\}, \quad k_a^* = (k_{11}/k_{33}) - 1 \text{ and}$$

$k_b^* = (k_{22}/k_{33}) - 1$, respectively.

From Eq. (20) and Eq. (21), one can easily recognize that the elastic anisotropy between $k_a$ and $k_b$ affects the effective diffusion anisotropy parameter $\sigma$. The value of the effective diffusion anisotropy $\sigma$ plays an important role in the formation of optical patterns. Considering both the intrinsically anisotropic distribution of the threshold intensity resulted from the elastic constant anisotropy of the NLC materials and the externally electric-tunable effective diffusion anisotropy, since it is related with the average tilt angle $\theta_a$ which is easily seen in Eqs. (19) and (20), one may employ different methods to obtain different optical patterns.

Generally speaking, if the value of $\sigma$ is positive, the value of $l_x$ is larger than that of $l_y$. This property makes the threshold intensity distribution has its minimum at $\varphi = \pi/2$ and maximum at $\varphi = 0, \pi$. Therefore once the input light intensity is above and near the minimum threshold, the vertical roll can be obtained since it will experience the maximum gain. On the other hand, when the input light intensity is above and near the maximum threshold, the hexagon is expected to be formed based on its compact structure. If the value of $\sigma$ is negative, the value of $l_x$ is smaller than that of $l_y$. This property makes the threshold intensity distribution has its minimum at $\varphi = 0, \pi$ and maximum at $\varphi = \pi/2$. Therefore, once the input

light intensity is above and near the minimum threshold, the horizontal roll can be obtained and once the input light intensity is above and near the maximum threshold, the hexagon is expected to be formed. The special case for $\sigma = 0$ represents the isotropic distribution of the threshold intensity and the hexagon can be obtained when the input light intensity is above and near the threshold.

On the basis of the above description, in order to verify the influence of the elastic constant anisotropy on optical pattern formation, it's straightforward to study the influence of the elastic constant anisotropy by considering the value of the effective diffusion anisotropy $\sigma$. On the basis of Eq. (20), in Table 3.1, we list the possible values of $\sigma$ for different regions of the elastic constant anisotropy. The material and system parameters used in the calculation are summarized in Table 3.2.
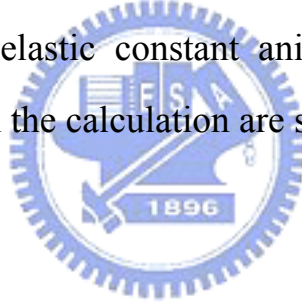
Table 3.1    Classification of regions according to the Frank elastic constant anisotropy.

| parallel planar-aligned | A $(k_a > 0, k_b > 0)$ | B $(k_a < 0, k_b < 0)$ | C $(k_a > 0, k_b < 0)$ | D $(k_a < 0, k_b > 0)$ |
|---|---|---|---|---|
| $\sigma > 0$ | $k_b/k_a < 0.11$ | $k_b/k_a > 1$ | All | None |
| $\sigma$ can be tuned to vanish | $0.11 < k_b/k_a < 1$ | $0.11 < k_b/k_a < 1$ | None | None |
| $\sigma < 0$ | $k_b/k_a > 1$ | $k_b/k_a < 0.11$ | None | All |

Table 3.2    The liquid crystal parameters, cell properties, and optical system parameters used in the calculations.

| liquid crystal material | E7 |
| --- | --- |
| $n_e$ | 1.75 |
| $n_o$ | 1.5231 |
| $\varepsilon_{//}$ | 19.6 |
| $\varepsilon_\perp$ | 5.1 |
| $k_{11}$ | 12 pN |
| $k_{33}$ | 19.5 pN |
| cell gap (d) | 68 $\mu$m |
| feedback length (L) | 1.9 cm |
| mirror reflectivity (R) | 0.65 |
| wavelength ($\lambda_0$) | 514.5 nm |

The value of $m$ versus the average orientational angle is plotted in Fig. 3.2. From Fig. 3.2 the value of $m$ is decreasing as the orientational angle increasing. Between the possible range of the average orientational angle $\theta_a$ from 0 to $\pi/2$, the value of $m$ is positive and has its maximum as 1 at $\theta_a$ = 0 and minimum as 0.11 at $\theta_a = \pi/2$. This means that we can modulate the value of m from 0.11 to 1 by controlling the average orientational angle $\theta_a$ electrically. For the region A in Table 3.1, the values of both $k_a$ and $k_b$ are positive and the value of $\sigma$ can be easily estimated from Eq. (21) and Fig. 3.2.
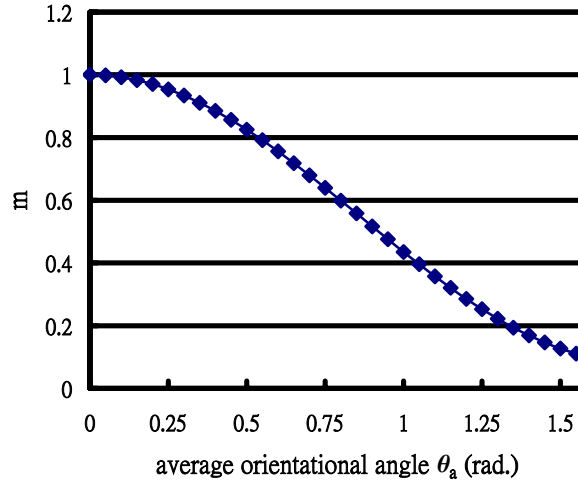
Fig. 3.2    The calculated value of m versus the average orientational angle $\theta_a$.

To more clearly illustrate the value of σ in this region (region A) we plot an example in Fig. 3.3(a). From Fig. 3.3(a), one can see that the value of σ is positive if $k_b/k_a < 0.11$, is negative if $k_b/k_a > 1$, and can be modulated to be zero by changing the value of m electrically in the range that $0.11 < k_b/k_a < 1$. For example when $k_b/k_a = 0.6$, one can have σ = 0 by tuning $\theta_a$ to have m = 0.61962. The possibility of modulating σ to zero by changing the value of m can be clearly seen when we plot the diffusion lengths in Eq. (19) and Eq. (20) in Fig. 3.4(a). From Fig. 3.4(a), one can see that the diffusion anisotropy can be canceled in the range $0.11 < k_b/k_a < 1$.
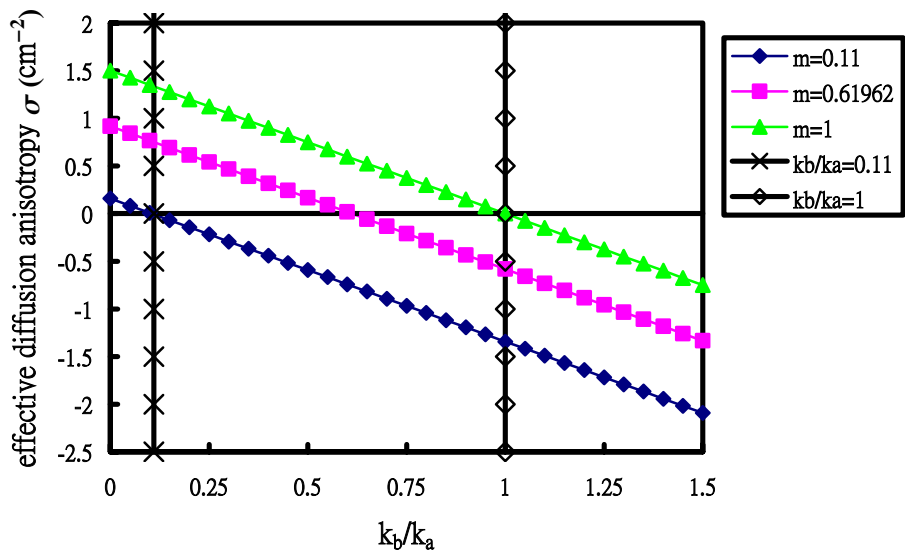
(a)
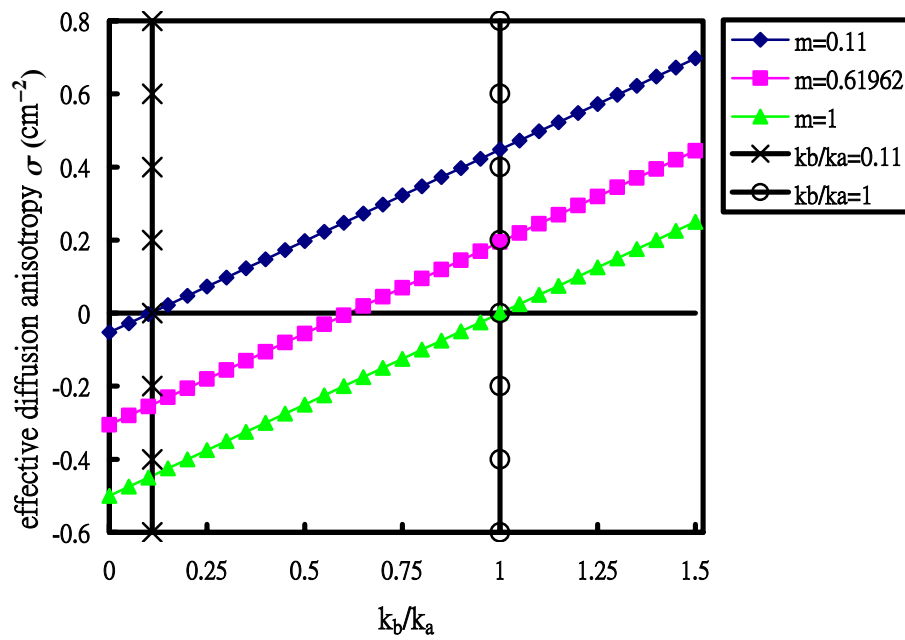


(b)

Fig. 3.3 The calculated effective diffusion anisotropy σ versus the elastic anisotropies. (a) for region A; with $k_a = 1.5$ (b) for region B; with $k_a = -0.5$.

(a)



(b)

Fig. 3.4 The calculated diffusion lengths versus the average tilt angle $\theta_a$. (a) for region A; with $k_a = 1.5$ (b) for region B; with $k_a = -0.5$. Please note that l$_x$ is the same for different $k_b/k_a$ if $k_a$ is not changed.

This means that the vertical roll, the horizontal roll and the hexagon can be expected to be obtained in region A by considering suitable elastic constant anisotropy range and employing suitable methods. For the region B in Table 3.1, the value of b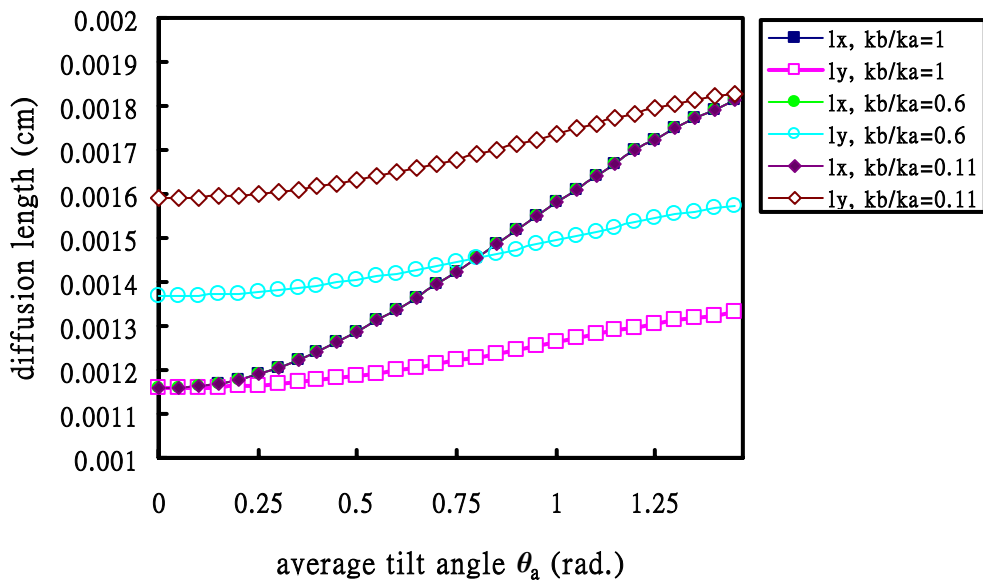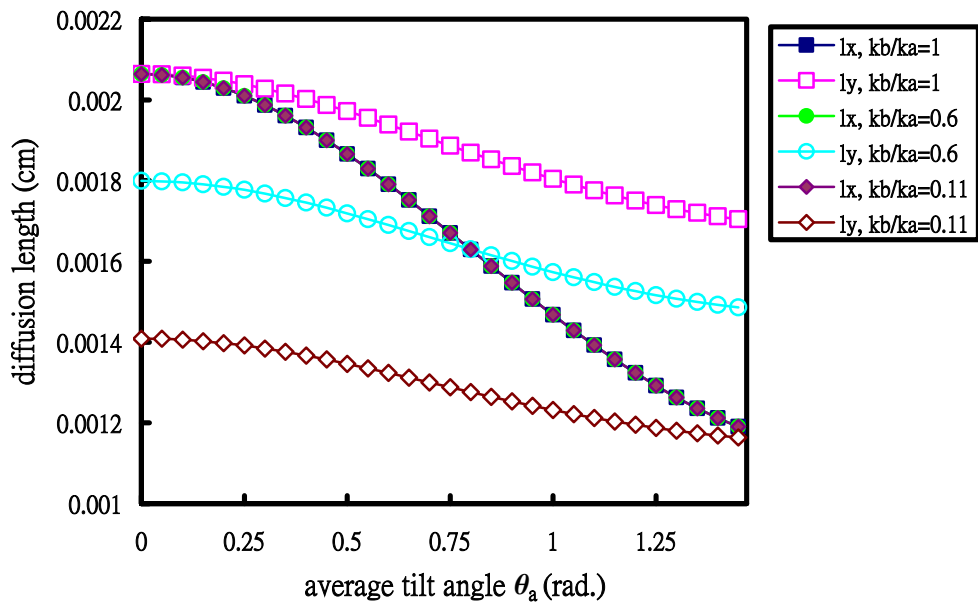oth $k_a$ and $k_b$ are negative. From Eq. (19) and Fig. 3.2, the value of $\sigma$ can also be easily estimated. We plot an example in Fig. 3.3(b) to see the value of $\sigma$. From Fig. 3.3(b), one can see that the value of $\sigma$ is positive for $k_b/k_a > 1$, is negative for $k_b/k_a < 0.11$, and can be modulated to be zero by changing the value of m electrically in the range that $0.11 < k_b/k_a < 1$. The possibility of modulating $\sigma$ to zero by changing the value of *m* can also be seen from the diffusion lengths plotted in Fig. 3.4(b). This means that the vertical roll, the horizontal roll and the hexagon can also be obtained by considering suitable elastic anisotropy range and employing suitable methods in this region.

A simple method to obtain the vertical roll, the hexagon and the horizontal roll can be suggested if the effective diffusion anisotropy $\sigma$ can be canceled electrically like the case in region A and B. For example, Figs. 3.5(a)-(c) show the results for $k_a = 0.625$ and $k_b/k_a = 0.512$ in region A. From Fig. 3.5(a) we find that $l_x$ and $l_y$ are equal at $\theta_a = 0.905$ radian and the threshold intensity distributions for all the azimuthal modes are the same at $\theta_a = 0.905$ radian as shown in Fig. 3.5(b). This property makes the formation of the stable vertical roll, the stable horizontal roll and the stable hexagon possible by simply modulating the average tilt angle electrically. The threshold intensity versus the azimuthal angles for several fixed tilt angles is shown in Fig. 3.5(c). If the input light intensity is about 55.6 W/cm$^2$ and $\theta_a$ is 0.85 radian, then the modes which are allowed to appear is closed to the minimum at $\varphi = \pi/2$ and thus the stable
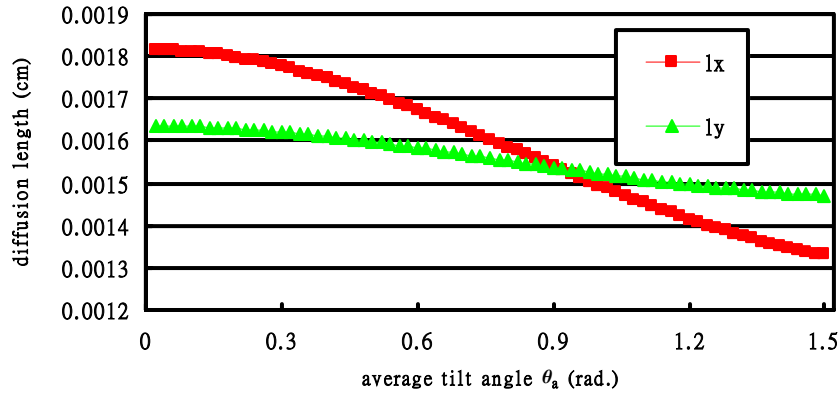
(a)
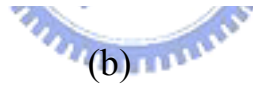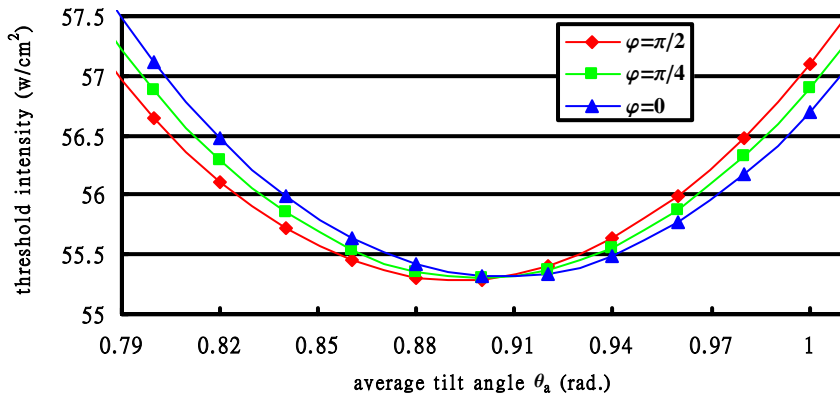


(b)
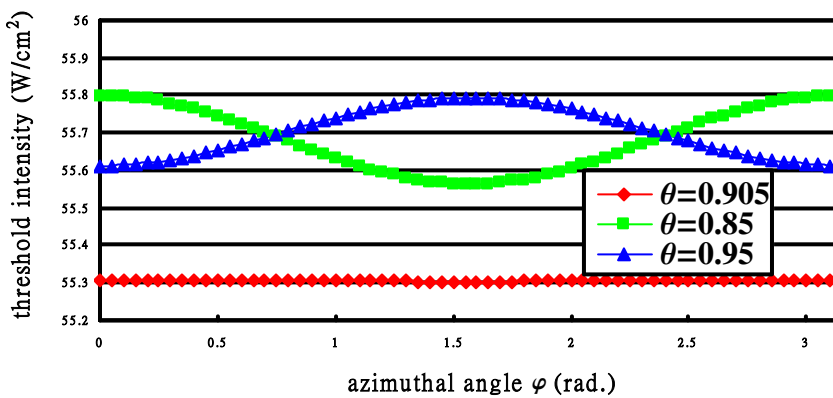


(c)

Fig. 3.5 (a) The calculated diffusion lengths versus the average tilt angle $\theta_a$ (b) The calculated threshold intensity versus the average tilt angle $\theta_a$ when the azimuthal angle $\varphi$ is fixed (c) The calculated threshold intensity versus the azimuthal angle $\varphi$ when the average tilt angle $\theta_a$ is fixed With $k_a = 0.625$, $k_b/k_a = 0.512$.

vertical roll is expected to be obtained. If $\theta_a$ is 0.905 radian, all the modes in different azimuthal $\varphi$ are allowed to appear and then the stable hexagon is expected to form due to its compact structure. If $\theta_a$ is 0.95 radian, the modes that are allowed to appear are closed to $\varphi = 0$ or $\varphi = \pi$. Therefore the stable horizontal roll is supposed to appear. This method to obtain different patterns is similar to the method used by Santamato by rotating the NLC sample in Ref. 11.

Now we continue to discuss the cases in regions C and D. One can easily realize from Eq. (21) and Fig. 3.2 that the value of $\sigma$ in region C is always positive and the value of $\sigma$ in region D is always negative. In region C, the value of $k_a$ is positive and the value of $k_b$ is negative. From Fig. 3.2, one can see that the value of $m$ is always positive and then the resulted value of $\sigma$ in region C is always positive. Similarly, in region D the value of $k_a$ is negative, the value of $m$ is positive and the value of $k_b$ is positive. Then the resulted value of $\sigma$ is always negative in region D. The examples of the threshold intensity distribution in regions C and D are plotted in Fig. 3.6(a) and (b), respectively. The possible optical patterns can be obtained in region C are the vertical roll and the hexagon, and in region D they are the horizontal roll and the hexagon.

As for the vertical-aligned case, the analysis can be easily done by following the similar procedure for the parallelly planar-aligned case. One just needs to replace $\theta_a$, $G$, $k_a$, and $k_b$ by $\beta_a$, $G^*$, $k_a^*$ and $k_b^*$, respectively and the results are similar.

From the above description, one can see that the Frank elastic constant anisotropy indeed plays an important role for optical pattern formation in the studied system. It is not easy to illustrate all the above cases

experimentally since the commercially available rod-like liquid crystal materials generally posses the property that $k_{33} > k_{11} > k_{22}$. Therefore, only the cases in region C for with parallelly planar-aligned LC films and the cases in region B with the vertical-aligned LC films may be obtainable now.



(a)
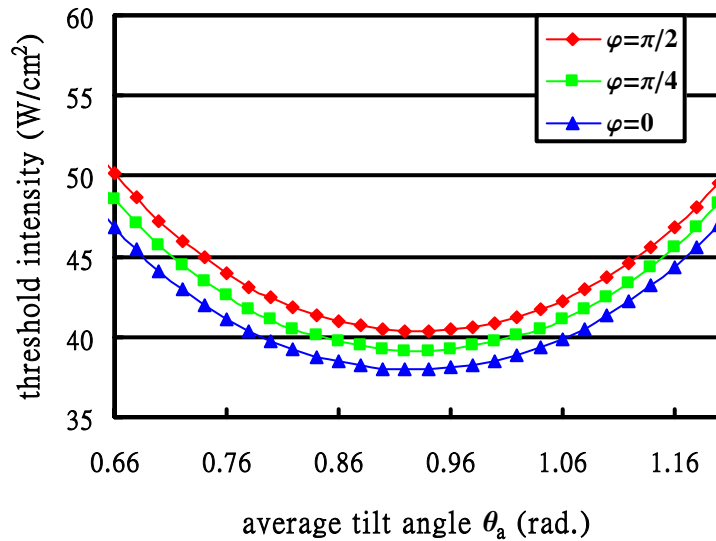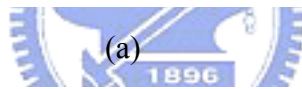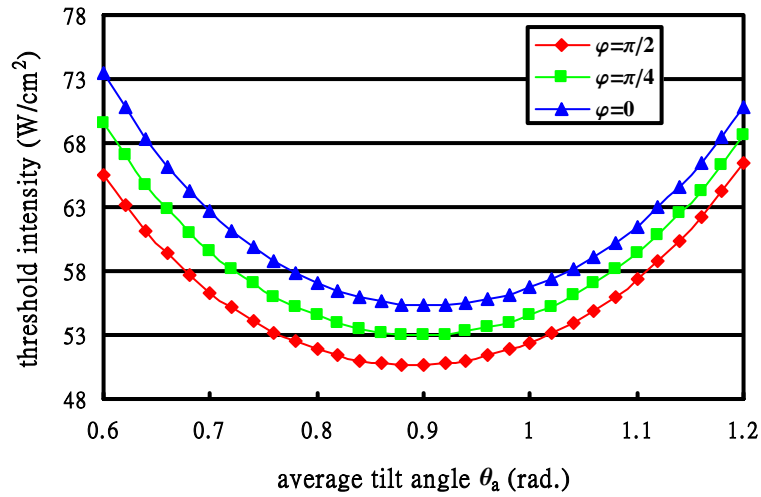


(b)

Fig. 3.6 (a) The calculated threshold intensity versus the average tilt angle $\theta_a$ when the azimuthal angle $\varphi$ is fixed; with $k_a = 0.625$, $k_b/k_a = -0.4$. (b)The calculated threshold intensity versus the average tilt angle $\theta_a$ when the azimuthal angle $\varphi$ is fixed with $k_a = -0.2$, $k_b/k_a = -1$.

3-3    Analysis of the influence of dielectric anisotropy of

nematic liquid crystals on optical pattern formation

phenomena

From Eq. (19), we can see that not only the anisotropy of the diffusion lengths is affected by the orientation of the liquid crystal molecules but also the effective nonlinearity is related with the orientation of the liquid crystal molecules. Therefore, once a positive dielectric anisotropy liquid crystal material is used and treated as the parallel-aligned configuration the orientation of the liquid crystal materials can be modulated by the externally applied electric field. Furthermore, the nonlinearity of the system can be modulated. In this subsection, we analyze the effect of the biasing voltage through the ability to change the nonlinearity by modulating the orientation of the NLC molecules electrically and see the influence on the optical pattern formation phenomena.

  Since the positive-dielectric-anisotropic NLC films are used the orientation of the liquid crystal directors is changed when the applied voltage exceeds the Freedericksz voltage $V_{th}$ (in our case $V_{th} = 0.9V_{rms}$). As an example, from Eq. (11) we plot the changing of $\theta_a$ with respect to the applied biasing voltage and is shown in Fig. 3.7(a). From Fig. 3.7(a), we can see that $\theta_a$ can be modulated by the applied biasing voltage. Therefore, from Eq. (17) we plot $\alpha$ with respect to $\theta_a$ as shown in Fig. 3.7(b). From Fig. 3.7(b), we see that $\alpha$ initially increases with $\theta_a$ increasing and reaches a maximum when $\theta_a$ is about 0.9 rad.. However, when $\theta_a$ is larger than 0.9 rad. $\alpha$ decreases with $\theta_a$ increasing.

Furthermore, the changing behavior of α with respect to $\theta_a$ directly affects the threshold intensity distribution when $\theta_a$ is changed.
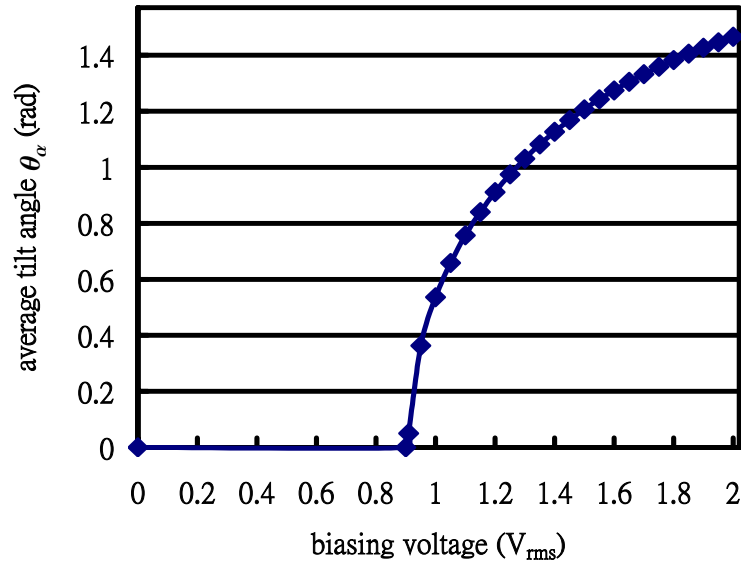


(a)
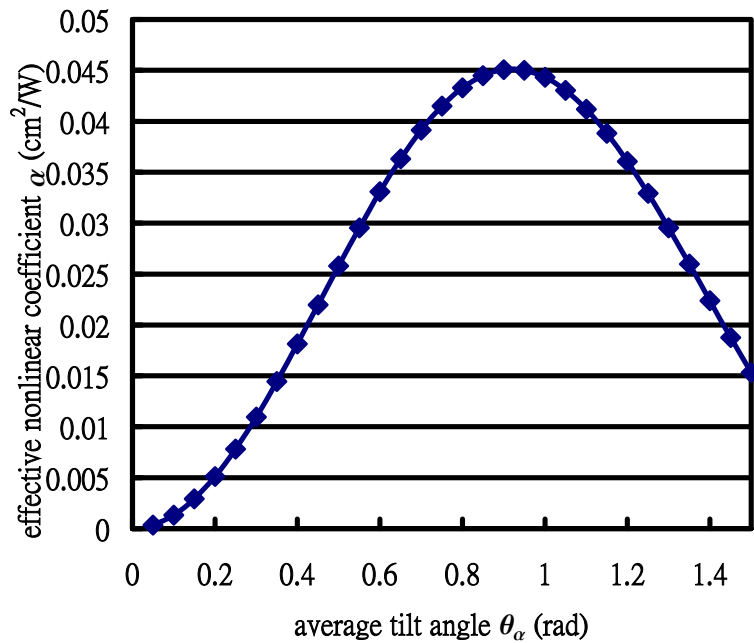


(b)

Fig. 3.7 (a) The calculated curve of the average tilt angle $\theta_a$ versus the biasing voltage (b) the effective nonlinear coefficient α

versus the average tilt angle $\theta_a$; with beam diameter=1.4 mm, d=68 μm, L=1.9 cm, R=0.65, input light power=0.91 W

(a)
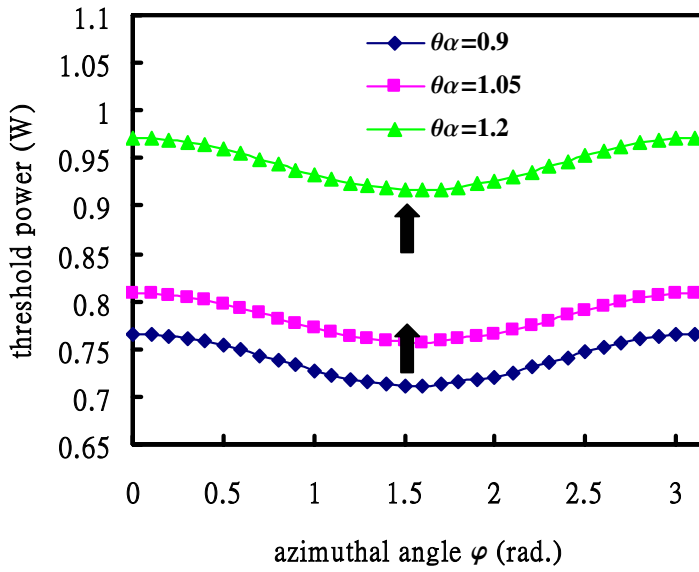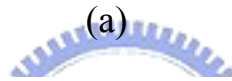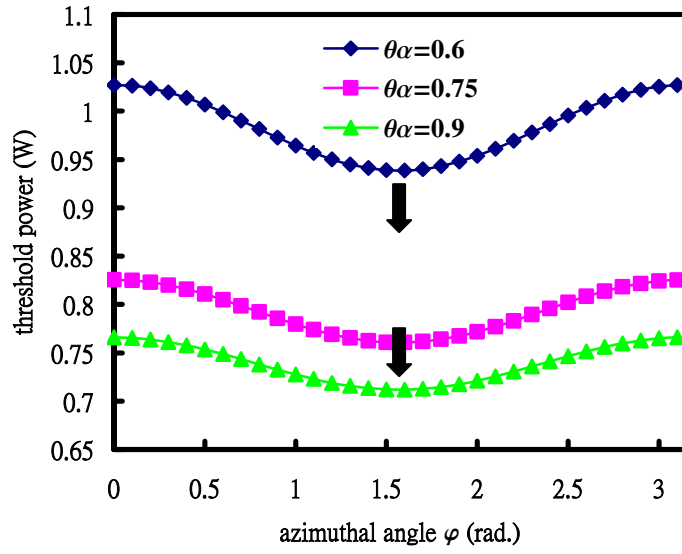


(b)

Fig. 3.8 (a) the calculated threshold power distribution for different $\theta_a$; from the top to the bottom are $\theta_a$ = 0.6, 0.75 and 0.9 rad, respectively (b) the calculated threshold power distribution for different $\theta_a$; from the bottom to the top are $\theta_a$ = 0.9, 1.05 and 1.2 rad, respectively; with beam diameter=1.4 mm, d=68 μm, L=1.9 cm, R=0.65, input light power=0.91W

Fig. 3.8(a) and 3.8(b) show the theoretical curves of the threshold power at different $\theta_a$. The threshold power is obtained by the product of Eq. (17) and the beam area. In our calculation the beam diameter is assumed to be 1.4 mm. From Fig. 3.8(a) and 3.8(b), one can see that the threshold power distribution decreases with $\theta_a$ increasing when $\theta_a$ is smaller than 0.9 radian and increases with $\theta_a$ increasing when $\theta_a$ is larger than 0.9 radian. Therefore, considering both the anisotropic distribution of the threshold intensity and the electric-modulated property of the effective nonlinear coefficient $\alpha$ an electric method to obtain different optical patterns can be expected. When $\theta_a$ is initially biased at a value smaller than 0.9 radian, one can input a light power larger than the maximum threshold (in our case the maximum locates at $\varphi = 0^0$ and $180^0$) the hexagon is expected to be formed based on its stable and compact structure. This is similar to that in the isotropic case and we can expect the oscillation of three ripple patterns leading to hexagons formation. Decreasing the biasing voltage, which decreasing $\theta_a$, results in the increasing of the threshold. Once the minimum threshold (in our case the minimum locates at $\varphi = 90^0$) is tuned below and near to the input light power, only the mode with the lowest threshold power will be enhanced and the roll pattern should be observed. On the other hand, when $\theta_a$ is initially biased larger than 0.9 radian one has to increase the biasing voltage to see the roll pattern.

# Chapter 4　Experiments

From the analysis in Chapter 3, we know that the intrinsic anisotropies of NLC materials indeed play important roles on the optical pattern formation phenomena. In this Chapter, we present the experimental results according to the analysis in Chapter 3.

## 4-1 Sample preparation, experimental setup and measurements
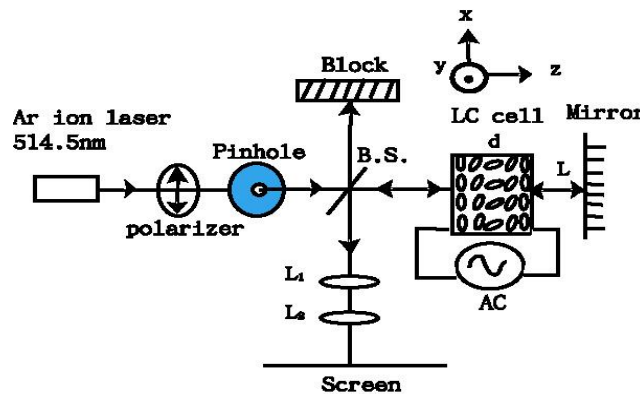


Fig. 4.1　Experimental setup: B.S., beam splitter; d, cell thickness; L, feedback length; LC, liquid crystal; L'i, lens

The experimental setup is the same as we shown in Fig. 2.2 and we redraw it as in Fig. 4.1. The Sample used in our experiment is a nematic liquid-crystal cell prepared by sandwiching the nematic E7 between two indium tin oxide-coated (ITO) glass windows that had been treated with polyvinyl alcohol (PVA) and achieved the parallelly planar alignment by rubbing. The nematic E7 is a mixed liquid crystal; it has many components. The material parameters of E7 including the temperature

range of nematic phase, refractive index, and elastic constants are listed in Appendix I as a reference. Different values of the parameters for E7 are obtained from different published sources because of the variations of different measuring methods. The thickness of the liquid-crystal cell is about 68 μm which is controlled by the calibrated Myler spacer and measured by using a micrometer. The sample area is about 2x2 cm$^2$ which is much larger than the laser-spot size of about 1.4 mm in diameter. The planar alignment quality is examined by microscopy and conoscopy to assure that there is no observable defects. The hyperbola conoscopic picture which shows the planar alignment is shown in Fig. 4.2.
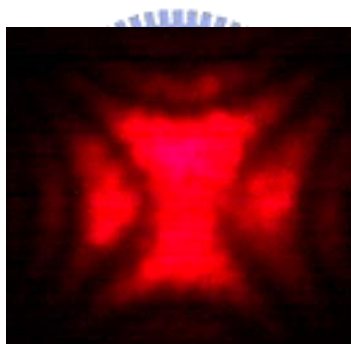


Fig. 4.2 Conoscopic picture for the planar aligned NLC sample.

The applied external fields include a 1kHz electric field and an optical field. The 1kHz electric field is generated by a microcomputer's waveform synthesizer (Quatech Inc., WSB-A12M) applied normally to the sample's glass windows and its amplitude could be programmably controlled. The laser beam used is from a CW Ar-ion laser (Spectra-Physics, Model 2080-15s) with wave length at 514.5 nm and linear polarization at TEM$_{00}$ mode. The original beam waist from the

Ar-ion laser is 1.9 mm and the input beam diameter is controlled by a pinhole of 1.4 mm in diameter. The pinhole is used to block the stray light in the low intensity wings of the beam and allows the high intensity region to pass through the sample. The reflectivity of our reflecting mirror is about 0.65. The distance between the sample and the feedback mirror is 1.9 cm. The lens $L_1$, $L_2$ are arranged to observe the near-field picture of the reflected beam impinging on the sample. A silicon photodetector system (UDT, Model S380), which is covered by an iris diaphragm to reduce the scattering noise recorded, is used to detect the input light power. The observed picture was recorded by a digital camera with its exposure time of 1/800 second. The ambient temperature is roughly controlled by using a mounted thermo-electric cooler for eliminating laser heating effect and keeping the liquid crystal in nematic phase.

## 4-2  Experimental observations

In the following, the experimental results will be separated as three parts to describe the anisotropic effects and the electrical-modulating effect.

## 4-2-1  Optical pattern formation in a parallelly planar-aligned NLC film

In considering the prediction by the results of the LSA of the governing diffusion-like equation, the optical pattern should be formed as the input

light intensity is above the threshold intensity. Although the distribution of the threshold intensity in our planar-aligned homogeneous NLC film is anisotropic and has the minimum at $\varphi=90^0$ and the maximum at $\varphi=0^0$ and $180^0$, we first fix the applied voltage at 1.117 $V_{rms}$ then input a light beam with power 0.83 W. From Eq. (11), the average tilt angle $\theta_a$ at this external field conditions is about 0.787 radian and the maximum threshold power obtained by the product of Eq. (17) and the beam area is about 0.8W as shown in Fig. 3.1(b). The near-field picture observed on the screen is shown in Fig. 4.3 and the stable hexagon is obviously formed.
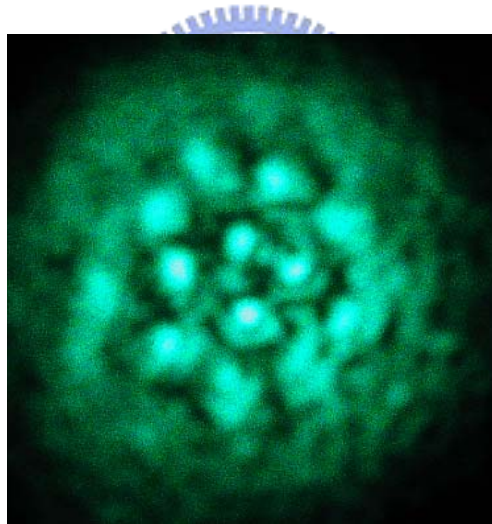


Fig. 4.3    Near-field pattern observed on the screen; input power=0.83 W, biased voltage=1.117 Vrms, d=68 $\mu$m, L=1.9 cm,

R=0.65, beam diameter=1.4 mm, and exposure time=1.25 ms.

## 4-2-2 Obtaining different optical patterns by the optical method

The optical pattern formation from our quasi-electric-field-biased planar-aligned NLC film has been confirmed as shown in Fig. 4.3. Considering the theoretical analysis in Chapter 3, the NLC (E7) film is classified in the region C in Table 3.1. The anisotropy between the diffusion lengths is always positive and the anisotropic distribution of the threshold power appears, as shown in Fig. 3.1(b) for example.

Therefore, in order to study the effects of the anisotropic distribution of the threshold power, we fix the biasing voltage at 1.117 $V_{rms}$ and change the input light power from 0.71 W to 0.98 W with a power step about 0.03 W. The input light power is measured after the beam passing through the pinhole and the beam splitter. In our experiments, the laser beam is blocked when we change the input light to the desired power. Therefore the pattern formations always start from the homogeneous state. We find that, as the input power is 0.74 W and 0.78 W the observed near-field pictures are the stable rolls as depicted in Fig. 4.4. Furthermore, as the input power is close to 0.8 W, the observed near-field picture are not stable and the patterns are appear as the roll and the hexagon alternately. The competition of the patterns is shown in Figs. 4.5(a)-(c).

(a)                                        (b)
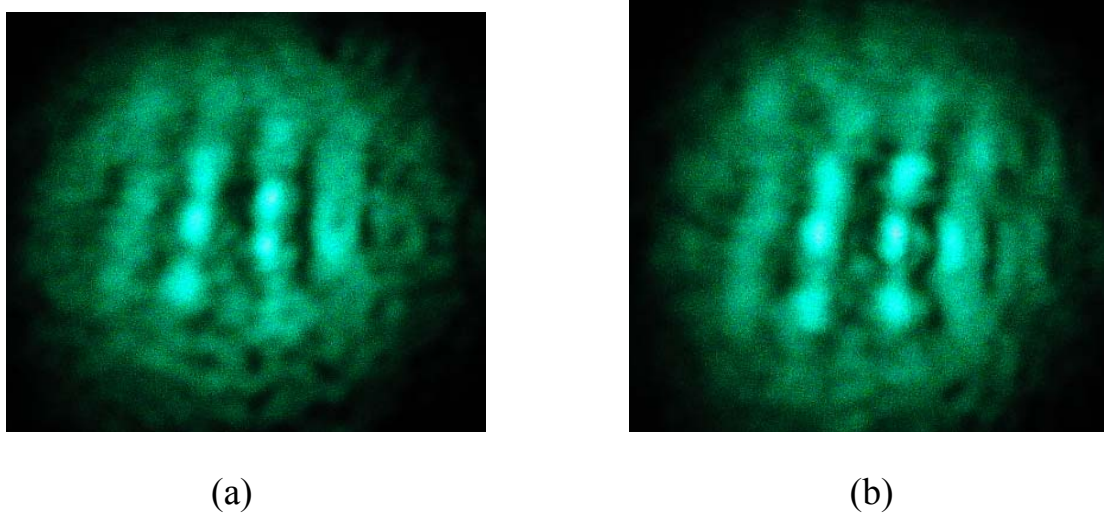
Fig. 4.4 Stable roll patterns observed on the screen (a) input power=0.74 W (b) input power=0.78 W



(a)                    (b)                    (c)
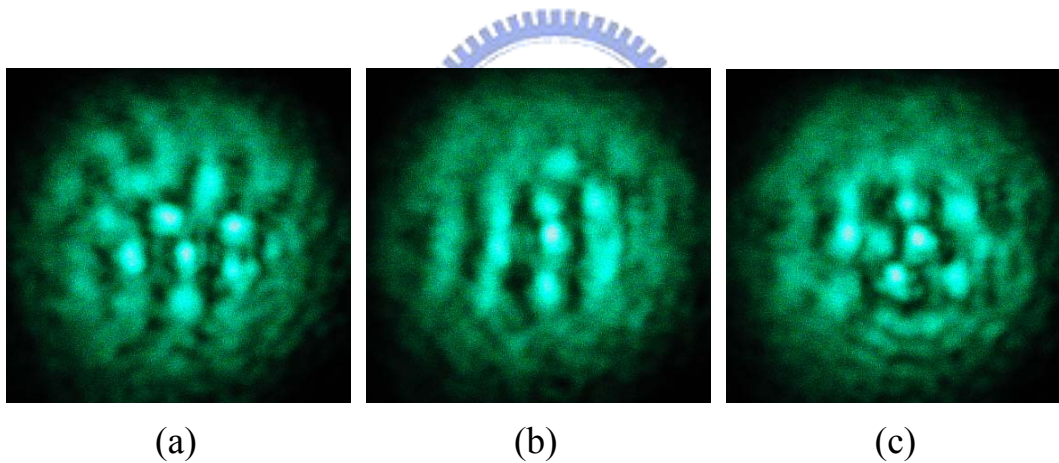
Fig. 4.5 Pattern sequence showing the competition between the roll and the hexagon patterns; input power=0.8 W.

As the input light power is at 0.83 W the stable hexagon is obtained, however, if the input light power increases continuously to about 0.98 W the pattern becomes unstable and turns chaotic finally. The hexagons and the chaotic patterns are shown in Fig. 4.6.

<div align="center">(a)                (b)</div>
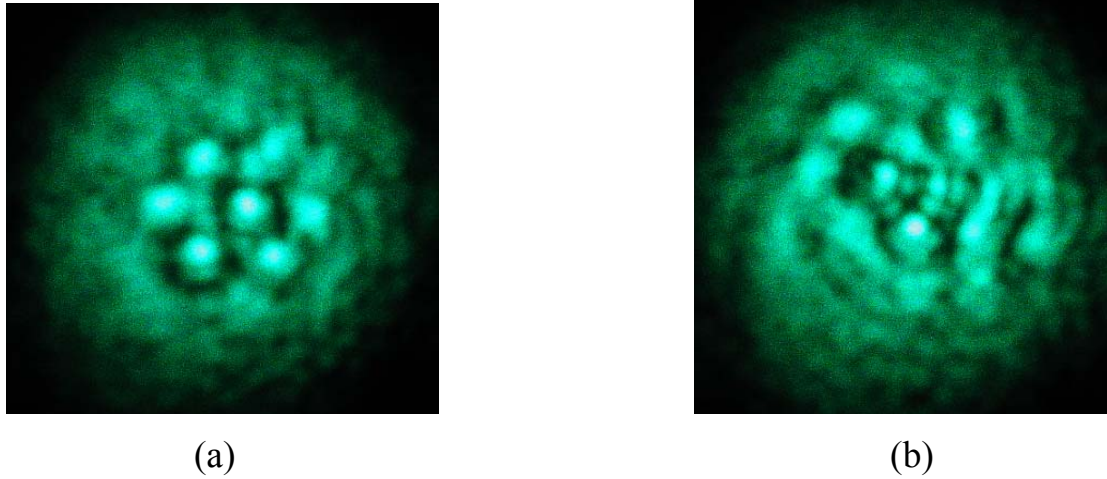
Fig. 4.6 Stable hexagon and chaotic patterns observed on the screen (a) input power= 0.83 W (b) input power= 0.98 W.

## 4-2-3 Obtaining different optical patterns by the electric method

In this subsection, we keep investigating the electric effect on the optical pattern formation phenomena. In the above experimental observations, we see that the different patterns can be obtained by changing the input light power. Here, we fix the input light power at 0.91 W and change the biasing voltage to see what patterns can be obtained.

Fig. 4.7 shows the pattern when the biasing voltage is zero. There is no structured pattern that can be identified. Obviously to create a significant optical pattern, a biasing voltage is required when a planar-aligned homogeneous NLC film is used.
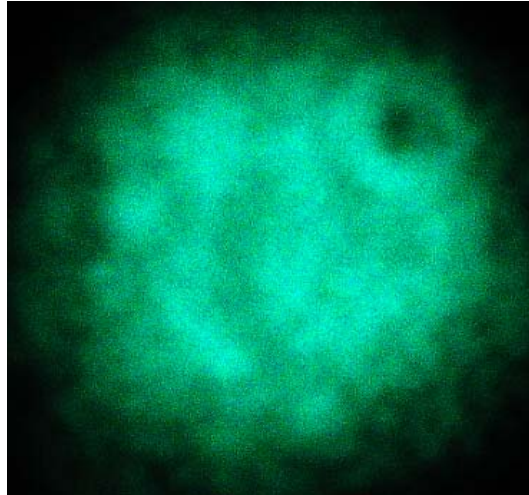
Fig. 4.7    Observed picture when the biasing voltage is zero with input light power= 0.91 W

In our experiments, we find that the patterns we get are similar to that we get by changing the input light power. The stable hexagons are obtained when the voltage is at 1.117 $V_{rms}$ and 1.114 $V_{rms}$ and are shown in Fig. 4.8.
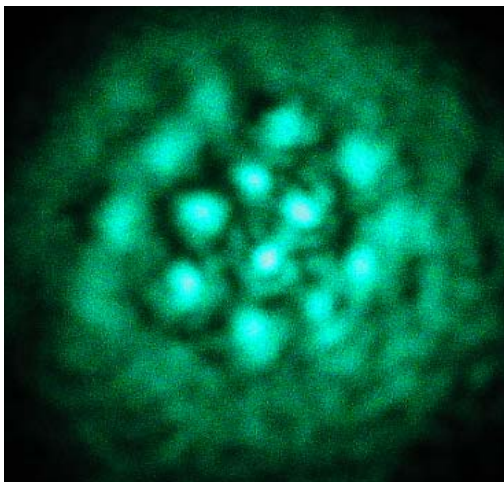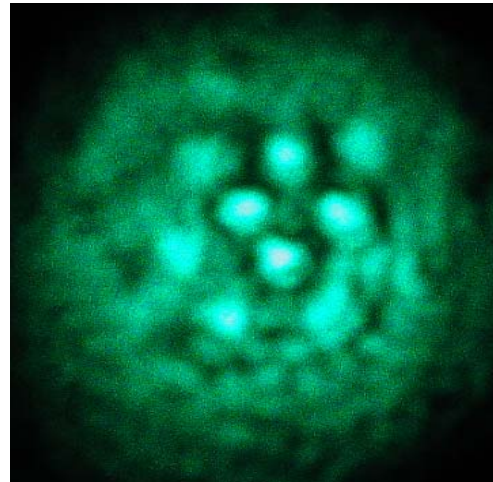


(a)                                        (b)

Fig. 4.8 Stable hexagon patterns observed on the screen (a) V= 1.117 $V_{rms}$ (b) V= 1.114 $V_{rms}$

The stable rolls are obtained when the voltage is at 1.032 V$_{rms}$ and are illustrated in Fig. 4.9. The pattern competition between the rolls and the hexagons is also observed when the biasing voltage is at 1.096 V$_{rms}$. See Fig. 4.10.
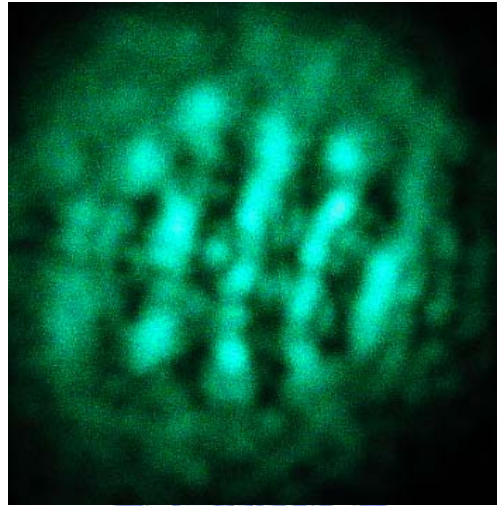


Fig. 4.9    Stable roll patterns observed on the screen; with V= 1.032 V$_{rms}$



(a)                        (b)                        (c)
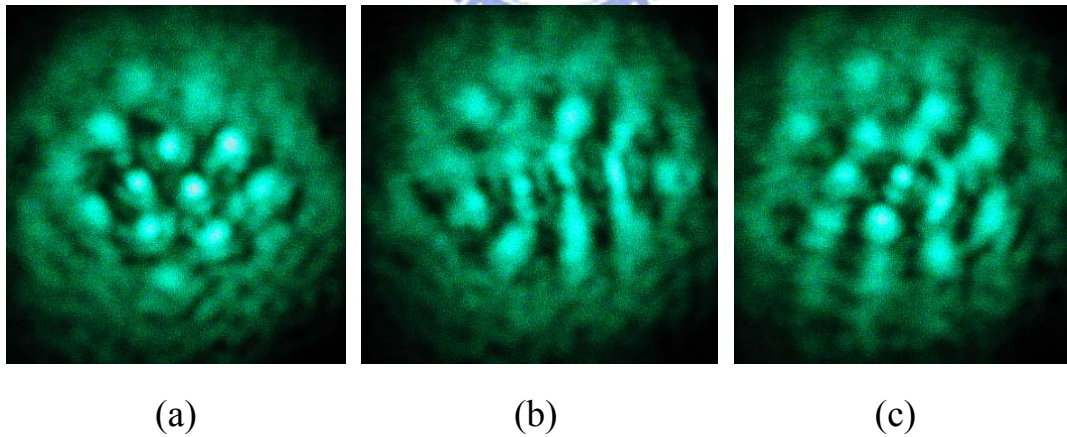
Fig. 4.10    Pattern sequence showing the competition between the roll and the hexagon patterns; V= 1.096 V$_{rms}$.

According to Santamato's explanation in Ref. 11, as the anisotropy between the diffusion lengths exists the roll patterns are expected to be seen and once the anisotropy is cancelled by rotating the sample at a

suitable angle the hexagon patterns are obtained. However, in our experiments, the hexagon patterns are seen even without canceling the anisotropy between the diffusion lengths. Not only the stable hexagons can be obtained but also the stable rolls are obtained by either changing the input light power or the biasing voltage. The pattern competition between the rolls and the hexagons is also observed when the input light power or the biasing voltage is between the values to obtain the stable rolls and the stable hexagons.

# Chapter 5    Discussion and Conclusions

In this chapter, we discuss the experimental results and compare them with the theoretical LSA results we get in Chapter 2. Finally, we make some conclusion about our work in this dissertation and we also suggest some future works which may be done in this topic about the optical pattern formation by using NLC films.

## 5-1 Discussion

From the experimental results we presented in Chapter 4, we observe the stable rolls, the stable hexagons and the competition between the rolls and hexagons. To investigate the relation between the patterns and the external fields, we plot the distribution of the threshold intensity (or power) to see the corresponding relations.

## 5-1-1  Discussion about the observed patterns obtained by optical method

In order to explain the experimental results described in Section 4-2-2, we substitute all values of the experimental parameters, including the cell parameters, the material parameters and the external fields, into Eq. (11) to obtain the average tile angle $\theta_a$ and into Eq. (17) to calculate the

threshold intensity distribution. Threshold power is calculated by the product of Eq. (17) and the beam area. When the biasing voltage is about 1.117 $V_{rms}$, the calculated average tilt angle $\theta_a$ is about 0.787 radian. We plot the calculated threshold power distribution versus the azimuthal angles in Fig. 5.1 to relate these experimental observations to our arguments from the theoretical results exhibited in Section 4-2-2. Even though the actual laser beam is a gaussian beam, for simplicity we calculate the threshold power from the threshold intensity shown in Fig. 3.1(b) by multiplying the beam area. Since only the light with high intensity passing through the pinhole and the sample the optical power with the peak intensity reaching the threshold intensity should be lower then that shown in Fig. 5.1. Nevertheless, it is clear that the stable rolls and stable hexagons exist and are obtained indeed in the power regions near the minimum and the maximum threshold power, respectively.
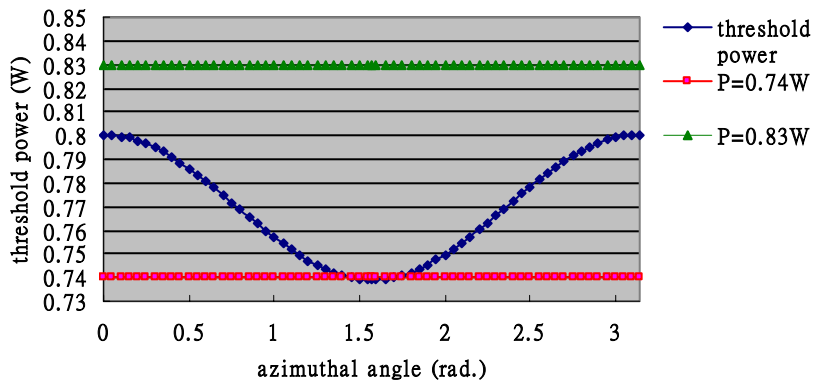


Fig. 5.1   The calculated curve of the threshold power versus the azimuthal angle φ when the average tilt angle $\theta_a$ is fixed at about 0.787 radian and the biased voltage is 1.117 Vrms.

According to the theoretical analysis and the experimental observations that we have shown above, one can see that the anisotropy indeed play an

important role in the formation of the rolls. Moreover, some more words have to be said about the input power issue. When the power is above the maximum threshold, the hexagons appear. However, chaotic patterns will be formed if we keep increasing the input power. One interesting question which may appear is that what patterns will be formed as the input power is between the minimum and the maximum threshold power. Actually our experimental observations at 0.77 W and 0.8 W indicate that the hexagons and the rolls may compete with each other and are not stable. This implies an interesting suggestion that the hexagons may still be formed without the requirement that all the modes with different azimuthal angles are allowed to appear. The experimental observations reasonably agree with the theoretical predictions discussed in Section 3-1.

## 5-1-2  Discussion about the observed patterns obtained by the electrical method.

In order to explain the experimental results we get in Section 4-2-3, following the same procedures in the preceding section, we insert the experimental parameters, including the cell parameters, the material parameters and the external fields values, into Eq. (11) to obtain the average tile angle $\theta_a$ and into Eq. (17) to calculate the threshold intensity distribution then obtain the threshold power by the product of Eq. (17) and the beam area. We obtain the results as illustrated in Fig. 5.2.
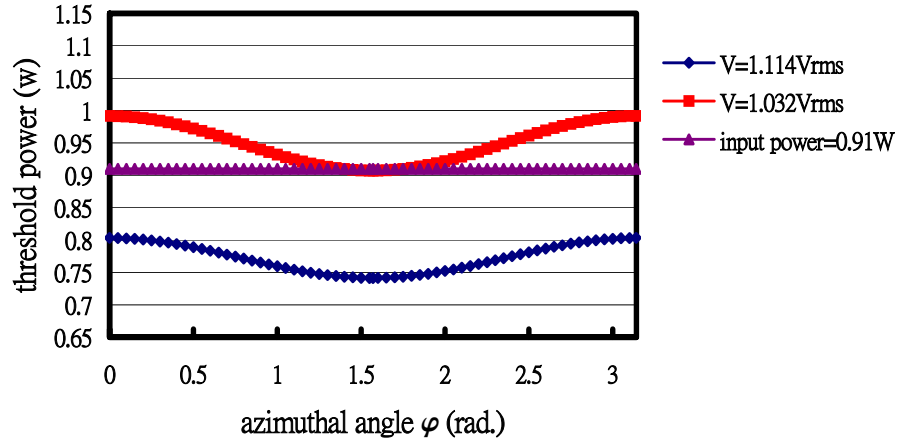
Fig. 5.2    The calculated curves of the threshold power versus the azimuthal angle φ, from the bottom to the top are biased voltage=1.114 $V_{rms}$ and 1.032 $V_{rms}$, respectively; the horizontal line indicates the input light power=0.91 W; with beam diameter=1.4 mm, d=68 µm, L=1.9 cm, R= 0.65.

Fig. 5.2 suggests that the stable hexagons are formed when the input light power is above and near to the maximum threshold, and the stable rolls are formed when the input light power is above and near to the minimum threshold. The competition between the rolls and the hexagons appear when the input light power is at some value between the maximum and the minimum thresholds.

In our calculation, we set the spatial frequency $q$ as $q \approx \pi / \sqrt{\lambda_0 L}$. The accuracy of such an approximation has been verified by measuring the relations between the feedback length and the pattern period. The pattern period for the feedback length $L$=1.9 cm is 198 µm and the theoretically predicted value is 197.74 µm. The experimental results agree with the theoretical predictions reasonably well.

## 5-1-3 Overall discussion

From the theoretical analysis and the experimental observations, the anisotropic properties of NLC materials indeed play important roles in the optical pattern formation. The orientation-dependent birefringence makes the pattern formation possible. The anisotropy of the elastic constant results in the anisotropic distribution of the threshold intensity for the patterns to be formed and this anisotropic distribution allows the observation of stable rolls and stable hexagons without using any external Fourier filter. Furthermore, the dielectric anisotropy of NLC materials enables to control the nonlinearity of the system by a small biasing voltage.

The pattern competition behavior between the rolls and hexagons we observed in our experiments is an interesting phenomenon worth continuing investigation. This dynamic behavior may associate with the dynamic property of the NLC molecules and with the instability of the roll state. The theoretical model we present here is only the instability analysis with respect to the homogeneous plane-wave state and the static state of the NLC molecules. Although only with the LSA results, the optical pattern formation phenomena can be effectively extended when the basic intrinsic properties are included.

The influence of the Talbot effect in this one-feedback-mirror system is also proved by measuring the period of the formed patterns.

## 5-2 Conclusions and future works

In this dissertation, we present the theoretical model to obtain the governing diffusion-like equation for both the orientation of the NLC directors and the Kerr-induced phase variation from the continuum theory for NLC materials for the one-feedback-mirror system to observe the optical pattern formation phenomena. The threshold intensity for the patterns to be formed is obtained from the linear stability analysis of the diffusion-like equation. Furthermore, the influences of the anisotropic properties of the NLC materials are analyzed.

The elastic anisotropy results in the anisotropic distribution of the threshold intensity. The anisotropic distribution of the threshold intensity is the key factor for the system to yield the pattern of stable rolls without using a Fourier filter. However, this does not imply that the hexagon patterns can not be obtained when the anisotropy of the threshold intensity distribution exists. The stable hexagons can still be obtained when the input light power is larger than the maximum threshold.

The anisotropic dielectric property of the NLC materials makes the modulation of the nonlinearity of the system possible by controlling the orientational distribution electrically. This property also facilitates the modulation of the formed patterns without changing the input light power.

The influences of the relative values of the Frank elastic constants are analyzed theoretically. We believe that once the material satisfying the elastic-constant requirement mentioned in Section 3-2 is available, the

method to obtain the vertical rolls, the horizontal rolls and the hexagons can be realized by simply modulating the biasing voltage.

The experimental results in our work qualitatively agree with the theoretical results well. The suggested forming properties in our theoretical analysis can be reasonably proved.

This work presented in this dissertation can be viewed as an opening of the study of the optical pattern formation phenomena from the point of view of the liquid crystal. We establish the theoretical model by using the simple linear stability analysis. The perturbation is added to the homogeneous plane wave state. However, the pattern competition phenomena we observed in our experiments are indeed associated with interaction of the roll and the hexagon patterns. Therefore, the stability analysis to the roll state can be included in the future studies.

Not only the instability analysis can be extended but also the dynamic behavior of the NLC molecules can be considered and it may become rather complicated.

Generally speaking, the study of the optical pattern formation phenomena is very interesting and the simple and tunable properties of liquid crystals can effectively be applied on the pattern formation phenomena and obtain interesting patterns without using Fourier filters. There still are many interesting topics which can be studied in the future, including both the theory and the experiments.

# References

1 P. G. De Gennes and J. Prost, *The physics of liquid crystals* (second edition) Chapter 1, Oxford University Press, New York, 1993.

2 F. Reinitzer, *Monatsh Chem.* **9**, 421 (1888)

3 O. Lehmann, *Z. Physikal. Chem.* **4**, 426 (1889). For a brief historical account of the early work see, H. Kelker and R. Hatz, *Handbook of Liquid crystals*, Verlag Chemie, Weinheim, Chapter 1 (1980)

4 G. Friedel, *Ann. Physique* **18**, 273 (1922)

5 W. J. Firth and C. Pare, Opt. Lett. **13**, 1096-1098 (1988)

6 G. Grynberg, Opt. Commun. **66**, 321-324 (1988)

7 W. J. Firth, J. Mod. Opt. **37**, 151-153 (1990)

8 E. V. Degtiarev and M. A. Vorontsov, J. Opt. Soc. Am. B **12**, 1238-1248 (1995)

9 R. Martin, A. J. Scroggie, G.-L. Oppo, and W. J. Firth, Phys. Rev. Lett. **77**, 4007-4010 (1996).

10 E. Benkler, M. Kreuzer, R. Neubecker, and T. Tschudi, Phys. Rev. Lett. **84**, 879-882 (2000).

11 E. Ciaramella, M. Tamburrini, and E. Santamato, Appl. Phys. Lett. **64** 3080-3082 (1994)

12 B. Gutlich, R. Neubecker, M. Kreuzer and T. Tschudi, Chaos **13**, 239-246 (2003).

13 R. Macdonald and H. J. Eichler, Opt. Commun. **89**, 289-295 (1992).

14 E. Ciaramella, M. Tamburrini, and E. Santamato, Appl. Phys. Lett. **63**, 1604-1606 (1993).

15 M. Tamburrini, M. Bonavita, S. Wabnitz, and E. Santamato, Opt. Lett. **18**, 855-857 (1993).

16 R. Neubecker, G.-L. Oppo, B. Thuering, and T. Tschudi, Phys. Rev. A **52**, 791-808 (1995).

17 D. Paparo, F. Castaldo, and E. Santamato, Chaos Solitons & Fractals **10**, 661-664 (1999)

18 S. H. Chen and Y. Shen, J. Opt. Soc. Am. B **14**, 1750–1753 (1997)

19 S. H. Chen and Y. Shen, Appl. Phys. Lett. **72**, 1281–1283 (1998)

20 Yuhren Shen, Hsu-Kuan Hsu, and Shu-Hsia Chen, J. Opt. Soc. Am. B **20**, 65-72 (2003)

21 Hsu-Kuan Hsu, Shu-Hsia Chen and Yinchieh Lai, Opt. Express **12**, 1320-1328 (2004)

22 Hsu-Kuan Hsu, Yinchieh Lai and Shu-Hsia Chen, submit to Jpn. J. Appl. Phys., (to be published)

23 Hsu-Kuan Hsu, Yinchieh Lai and Shu-Hsia Chen, submit to Appl. Phys. Lett., (revised)

# MERCK

| Mixture: | E7 |
|---|---|
| $S \rightarrow N$ [°C] | <−30 |
| Clearing point [°C] | +58 |
| | |
| Rot. visc. $\gamma_1$ [mPa·s]   (20 °C) | − |
| Viscosity [mm$^2$s$^{-1}$]         20 °C | 39 |
| Viscosity [mm$^2$s$^{-1}$]          0 °C | 145 |
| Viscosity [mm$^2$s$^{-1}$]       −20 °C | 1200 |
| Viscosity [mm$^2$s$^{-1}$]       −30 °C | 6400 |
| Viscosity [mm$^2$s$^{-1}$]       −40 °C | − |
| | |
| $n_e$              (589nm, 20 °C) | 1.7464 |
| $\Delta n$              (589nm, 20 °C) | +0.2253 |
| | |
| $\Delta \epsilon$              ( 1 kHz, 20 °C) | +13.8 |
| $\epsilon_{\parallel}$              ( 1 kHz, 20 °C) | 19.0 |
| | |
| $K_3/K_1$              +20 °C | 1.54 |
| $K_3/K_2$              +20 °C | − |
| | |
| $V_{(10,45,20)}$ [V] | 1.05 |
| | |
| $V_{(10,0,20)}$ [V] | 1.41 |
| $V_{(50,0,20)}$ [V] | 1.63 |
| $V_{(90,0,20)}$ [V] | 1.99 |
| | |
| Temp. dep. [mv/°C](0 − 40 °C) | 11.2 |
| Temp. dep. [%/°C](0 − 40 °C) | 0.80 |
| | |
| $(V_{50}/V_{10} - 1)·100$ [%] | 15.2 |
| $(V_{90}/V_{10} - 1)·100$ [%] | 40.6 |
| | |
| M 20 | 1.90 |
| M 0 − 40 | 2.53 |
| M' 0 − 40 | 1.89 |

# Curriculum Vita

基本資料：

姓　　名：徐旭寬

現在住址：苗栗縣苗栗市福安里 10 鄰中華路 592 號

實驗室地址：新竹市國立交通大學光電工程研究所液態晶體實驗室

電　　話：037-261213

實驗室電話：03-5712121 轉 56344

生　　日：民國 64 年 12 月 22 日

籍　　貫：台灣 苗栗

婚姻狀況：未婚

學　　歷：

學　　士：國立成功大學物理學系　　　民國 87 年 6 月

碩　　士：國立交通大學光電工程研究所 民國 88 年 8 月直升博士班

博　　士：國立交通大學光電工程研究所 民國 93 年 6 月


Publication List


Journal Papers:


1. Yuhren Shen, Hsu-Kuan Hsu and Shu-Hsia Chen, "Phase-conjugate

reflection and self-starting optical phase-conjugate oscillation in planar nematic liquid-crystal cells," J. Opt. Soc. Am. B, Vol. 20, No. 1, pp. 65-72 (2003)

2. <u>Hsu-Kuan Hsu</u>, Shu-Hsia Chen and Yinchieh Lai, "Crucial effects of the anisotropy on optical field induced pattern formation in nematic liquid crystal films," Opt. Express, Vol. 12, No. 7, pp. 1320-1328 (2004)

3. <u>Hsu-Kuan Hsu</u>, Yinchieh Lai and Shu-Hsia Chen, "Quasi-static electric-field-modulated optical pattern transition in a thin nematic liquid-crystal film with a single feedback mirror," submit to Appl. Phys. Lett. (revised)

4. <u>Hsu-Kuan Hsu</u>, Yinchieh Lai and Shu-Hsia Chen, "Influence of the Frank Elastic Constant Anisotropy on the Optical Pattern Formation through Nematic Liquid Crystal Films," Jpn. J. Appl. Phys. (accepted)

5. <u>Hsu-Kuan Hsu</u>, Shu-Hsia Chen and Ching-Hsiang Hsu, "Experimental observations of different-periodic interference patterns of scattering light by using an electric-field biased nematic liquid-crystal film," will submit to Opt. Express.

## Conference papers:

1. <u>Hsu-Kuan Hsu</u>, Ching-Hsiang Hsu and <u>Shu-Hsia Chen</u> , "Electric effects on the interference patterns of scattering light induced by orientational fluctuations," 2000 國際華人液晶研討會論文集, 成功大學, p. 98, 2000.

2. <u>Hsu-Kuan Hsu</u>, Ching-Hsiang Hsu and <u>Shu-Hsia Chen</u>, "Observation of the interference patterns of scattering light induced by orientational fluctuations in nematic liquid crystals," 21 世紀光電科技的趨勢與挑戰專題講座暨研討會論文集,交通大學, p. 76, 2001.

3. <u>H. K. Hsu</u>, C. H. Hsu and S. H. Chen, "Optical scattering patterns from nematic liquid crystal films with an external electric field," 2002

台灣光電科技研討會論文集 PE1-5.

4. <u>Hsu-Kuan Hsu</u>, Ching-Hsiang Hsu and <u>Shu-Hsia Chen</u>, "Different periodic changes of the scattering light interference patterns modulated by external electric and optical fields in nematic liquid crystals," 物理年會，中央研究院，物理雙月刊(二十五卷一期), p. 199, 2003 年 2 月

5. <u>Hsu-Kuan Hsu</u>，Shu-Hsia Chen and Yinchieh Lai "Observation of pattern formation in a thin quasi-static electric field biased nematic liquid crystal film with a single feedback mirror," 2003 台灣光電科技研討會論文集三 PF1-1.

6. Yinchieh Lai, <u>Hsu-Kuan Hsu</u> and Shu-Hsia Chen " Optical Pattern Formation through Nematic Liquid Crystal cells," 2003 年中國液態晶體學會年會暨研討會論文集 p. 2, 2003 年 12 月

7. <u>Hsu-Kuan Hsu</u>, Yinchieh Lai and Shu-Hsia Chen "Electrically modulated optical pattern transition in a thin nematic liquid crystal film with a single feedback mirror," 物理年會,清華大學,物理雙月刊(二十六卷一期), PE-28, p. 236, 2004 年 2 月